AN EXAMINATION OF RELATIONSHIPS BETWEEN MITOCHONDRIAL STRESS AND MUSCLE HEALTH IN A MODIFIED MOUSE MODEL OF EXPERIMENTAL AUTOIMMUNE MYOSITIS.

MADISON GARIBOTTI

A THESIS SUBMITTED TO

THE FACULTY OF GRADUATE STUDIES

IN PARTIAL FULFILLMENT OF THE REQUIREMENTS

FOR THE DEGREE OF

MASTER OF SCIENCE

GRADUATE PROGRAM IN KINESIOLOGY

YORK UNIVERSITY

TORONTO, ONTARIO

August 2023

ABSTRACT

Myositis is a rare autoimmune disorder characterized by skeletal muscle inflammation and weakness. Recently, mitochondrial stress has emerged as a possible disease contributor. To assess the relationship between mitochondrial stress and myopathy in myositis, evaluations of experimental models are required. Several models utilize an exotoxin, pertussis toxin(PT), coupled with foreign myosin injections. However, PT induces systemic inflammation impacting the ability to determine if the inflammatory response is consistent with myositis or a systemic response. Thus, the purpose of this thesis is to establish a modified myositis model whereby PT is excluded to exemplify the human condition, and to explore mitochondrial stress and myopathy. This modified model demonstrated no muscle atrophy occurred, but both the diaphragm and tibialis anterior(TA) displayed indices of mitochondrial stress. Additionally, the TA exhibited weakness that recovered over time. Suggesting the modified myositis model may induce a mild phenotype, highlighting the need for more robust model development.

ACKNOWLEDGEMENTS

First, I would like to thank my supervisors, Dr. Christopher Perry and Dr. Ali Abdul-Sater. They both have provided me with continuous guidance throughout the course of this degree and I will always be grateful for all of their patience. I want to extend a specific thanks to Dr. Perry for meeting with me for hours at a time (and I do mean hours) while I was still considering if a master's degree was the correct next step for me. I am beyond grateful for all the opportunities that never seem to stop, and I am so excited for all the opportunities that are still to come!

I, of course, could not get to this point without the help of my outstanding lab members and friends, Arshdeep, Luca, Shahrzad, Catherine, and Shivam. I am very grateful to say that I have made lifelong friends who always answer my one million and a half questions, no matter how ridiculous. Thank you for always being there to provide a joke, a helping hand, or put up with me and not complaining about how loud I am (rarely complaining). Arshdeep and I worked side-by-side throughout this degree, and I will always cherish all of our late night, early morning, and weekend lab memories together and thank you for everything. These few years have been amazing, and I can't wait to see what the next four years bring!

Table of Contents

List of Tables

List of Figures

List of Appendices

List of Abbreviations

-Cr	Absence of Creatine
+Cr	Presences of Creatine
ADP	Adenosine Diphosphate
ATP	Adenosine Triphosphate
CFA	Freund's Complete Adjuvant
CK	Creatine Kinase
DIA	Diaphragm
DM	Dermatomyositis
EAM	Experimental Autoimmune myositis
ETC	Electron Transport Chain
GCI	Glycerol CFA/IFA Group
GS	Glycerol Saline Groups
H_2O_2	Hydrogen Peroxide
IBM	Inclusion Body myositis
IFA	Freund's Incomplete Adjuvant
IFN-γ	Interferon Gamma
IIM	Idiopathic Inflammatory Myopathy
IL-1β	Interleuken-1 beta
IL-6	Interleuken-6
ILD	Interstitial Lung Disease
IM	Inner Membrane
IMNM	Immune Mediated Necrotizing Myopathy
IMS	Inner Membrane Space
M	Myosin Group
MCP-1	Monocyte Chemoattractant Protein-1
mH_2O_2	Mitochondrial Hydrogen Peroxide Emissions
MHC	Myosin Heavy Chain
mito-DAMP	Mitochondrial Damage-associated molecular Patterns
MSA	Myositis specific autoantibodies
mtCK	Mitochondrial Creatine Kinase
NADH	Nicotinamide Adenine Dinucleotide
NLRP3	Nucleotide-binding domain, leucine-rich-containing family, pyrin domain-containing-3 Inflammasome
NOX	NADPH Oxidase
OM	Outer membrane

OXPHOS	Oxidative Phosphorylation
Pi	Inorganic Phosphate
PM	Polymyositis
PMF	Proton Motive Force
PmFB	Permeabilized Muscle Fiber Bundles
PT	Pertussis Toxin
ROS	Reactive Oxygen Species
SOD	Superoxide Dismutase
STAT3	Signal transducer and activators of transcription 3
TA	Tibialis Anterior
TCA	Tricarboxylic acid cycle
TNF-α	Tumor necrosis factor-alpha

CHAPTER 1: INTRODUCTION

Autoimmune myositis is part of a group of autoimmune conditions that display various symptoms also known as idiopathic inflammatory myopathies (IIM). There are four common types of myositis, with the most common symptoms of these myopathies being muscle weakness, fatigue, and elevated muscle enzymes in serum[1]. While the mechanism of how these myopathies induce an autoimmune response resulting in muscle weakness is unknown, current treatment options vary depending on the type of myositis. Some examples of treatments include antimalarials (hydroxychloroquine), glucocorticoids and other immunosuppressants (Methotrexate, Azathioprine), intravenous immunoglobulin, biologic modifiers (Anti-TNF), Rituximab (Arava, alemtuzumab), supplements (creatine, turmeric curcumin), exercise as well as physical therapy[2]. There are no cures for any type of the idiopathic inflammatory myopathies; thus, treatment options are dependent on the patient's case in an attempt to suppress and mediate symptoms[2]. There are no direct therapy options for patients which results in patients receiving combinations of medications that have varying side effects further impacting patient welfare. Some side effects of the above-mentioned treatments include bone loss, susceptibility to infections, mood changes, liver toxicity, gastrointestinal symptoms, weakness, worsening skin conditions, rapid weight gain, and slow healing. As such, there is a need for therapy development to help provide additional treatment options for patients. In order to guide the development of new therapies for patients, experimental animal models of this disease are utilized to explore this condition entirely. One such model is the experimental autoimmune myositis (EAM) mouse model, which demonstrates immune cell infiltration within skeletal muscle, much like what is exhibited in skeletal muscle biopsies from patients. This animal

model is currently used in the literature, with recent literature suggesting myositis triggers a stress response in skeletal muscle mitochondria[3].

In the EAM model, mice are inoculated against a foreign (foreign to host) myosin protein injected with a pertussis toxin (PT) and adjuvant. When an adjuvant and PT are used in tandem, they are known to have additive effects. There are uncertainties over whether this approach consistently replicated autoimmunity seen in myositis, distinct from generalized muscle inflammation. Furthermore, the use of PT in research is increasingly discouraged by governing bodies[4]. It is arguably far removed from the process by which myositis may develop in a human, given that such toxins are not involved in the known etiology of this disease. As such, determining whether autoimmune myositis can be achieved in a mouse model without PT could help refine pre-clinical research approaches by avoiding potential generalized inflammation from toxin exposure in a sustainable manner with potential changes in future governing policies for animal research. Furthermore, some EAM models inject myosin into a mouse strain (*SJL/J*) that is known to develop a spontaneous myopathy resulting in a decrease of dysferlin protein due to a gene mutation[5]. Although this publication reported indices of muscle inflammation consistent with myositis, it is unclear whether this model was autoimmune myositis or an accelerated dysferlin myopathy[6]. The use of PT in this model also raises the uncertainty over whether the measures were a generalized inflammation or true autoimmunity, as autoantibodies associated with the human condition of myositis were not present in PT-induced EAM[7]. Therefore, it remains unclear if the EAM model of myositis can be developed in the absence of pertussis toxin and in a wild-type mouse that does not have genetic predispositions to myopathies. Furthermore, the degree to which myositis in the EAM model is consistent across muscle types and across time following multiple myosin inoculations remains unclear.

While autoimmunity is a complex process that requires further investigation in the context of myositis, understanding additional secondary contributors to this myopathy could guide therapy development. For example, mitochondrial stress has been identified in patients and a mouse model of myositis[3]. However, the degree to which mitochondrial ATP synthesis or reactive oxygen species (ROS) generation is altered across time and between muscle types in myositis remains unknown. Furthermore, the precise metabolic pathways regulating these processes have not been identified. Elucidating a potential role of mitochondrial stress could provide further insight into causes of muscle weakness in this disease.

CHAPTER 2: LITERATURE REVIEW

2.1 Introduction to Myositis

2.1.1 *Overview of Myositis*

Myositis is part of a heterogeneous group of immune-mediated diseases that are characterized by muscle weakness, elevated muscle enzyme levels (creatine kinase), and myopathic electromyographic evaluations[8]. Myositis is often expressed as one of four common types: dermatomyositis, polymyositis, immune-mediated necrotizing myopathy, and inclusion body myositis. Each type results in different manifestations of the disease and has different diagnostic markers in patients.

2.1.2 *Clinical manifestation/diagnostic features and treatment options*

Dermatomyositis (DM)

Dermatomyositis is one of the IIMs and can present at any age. Classic manifestations of DM are progressive proximal symmetrical weakness, elevated muscles enzymes, abnormal electromyogram, an abnormal muscle biopsy, with the most identifiable symptom being the presences of a cutaneous disease[9]. Characteristic rashes of DM occur at any time of the disease progression, like Gottron's papules which is a hallmark sign of DM. Erythematous lesions are found on joints of the hands, elbows, knees, and can accompany scaling[10]. Additional hallmark skin conditions include heliotrope rash, which consists of erythema (redness caused by inflammation) of the eyelids making them look discoloured almost purple[11,10]. Other skin conditions that are not solely signs of DM like livedo reticularis (crust and lesions in area of intense inflammation), telangiectatic macules (papules and lesions on the skin)[11]. Additional skin manifestation can include panniculitis (inflammation of subcutaneous fat), alopecia, flagellate erythema (linear streaks on back), poikiloderma (pattern of hyperpigmented and

hypopigmented macules), and calcinosis (calcium salt deposits in the skin and subcutaneous tissues)[11]. A characteristic unique to only DM is any form of skin manifestations, DM and PM are closely related with a higher risk of cancer development in both DM and PM[12]. Diagnostic approaches for DM can include muscle or skin biopsies but are not entirely necessary when evaluations of clinical symptoms and laboratory findings provide sufficient information. Determining the presences of myositis-specific autoantibodies (MSA) like anti-Jo-1 are evaluated in the diagnostic processes, other MSAs associated with DM are in ***Table 1***.

Polymyositis

Polymyositis (PM) is known to be closely related with DM[12], characteristic symptoms include symmetrical and proximal limb weakness, with distal muscle only being impacted in late stages of disease onset[12]. Neck muscle involvement is rare but does occur resulting in dropped head[12]. Though rare, cardiac involvement was found to be the cause of death in 10-20% of long-term cases[12]. This cardiac involvement can include arrhythmia, conduction abnormalities, cardiac arrest, congestive heart failure, myocarditis, and secondary fibrosis[12]. PM is the hardest myositis to diagnose as it can be mistaken for other clinical and pathological conditions like neuromuscular disorders, myotoxic exposure, endocrine diseases, muscular dystrophies, other forms of myositis (IBM or IMNM), and infections[12]. If other conditions are excluded, histopathology is the most effective form of diagnosis but many re-diagnostic testing have identified that 36% of originally diagnosed PM cases were actually connective tissue disease or IBM at about 26 %[12]. Though PM and DM share many similar autoantibodies, some MSAs that are more common in PM are outline in ***Table 1***.

Immune-mediated necrotizing myopathy

Clinical features of immune-mediated necrotizing myopathy (IMNM) are the presence of proximal muscle weakness and high creatine kinase levels[13]. Aggressive manifestations of IMNM are directly related to the type of autoantibody that is expressed. Anti-SRP positive IMNM has an increased chance of developing interstitial lung disease (ILD), and higher risk of cardiac involvement, but in anti-HMGCR positive IMNM there is a decreased likelihood of developing ILD and less chance of cardiac involvement[13]. Diagnosis of IMNM tests MSAs using an ELISA test, in some cases that do not present MSA a muscle biopsy is required, but much like PM and DM diagnosis of patients requires a variety of testing and is case specific[13]. The MSAs that are more common in IMNM are outline in ***Table 1***.

Inclusion body myositis

Inclusion body myositis (IBM) is more common in middle or late aged individuals, and manifests as difficulty walking or using their hands due to weakness of finger flexors or knee extensors[14]. Dysphagia is an under-reported symptom, but becomes more evident with disease progression and can cause nutritional deficiency, weight loss, and aspiration pneumonia which are causes of mortality in IBM[14]. The major area of muscular involvement in IBM are weakness of elbow flexion, shoulder abduction, forearm muscle controlling finger flexing, ventral forearm atrophy, knee extensor weakness, as well as vastus medialis and lateralis weakness[14]. IBM is often misdiagnosed due to age or arthritis, but laboratory tests showing abnormal levels of creatine phosphokinase, and evaluations of autoantibodies can identify IBM[14]. The MSAs that are more common in IBM are outline in ***Table 1***.

There is currently no cure for myositis with vary symptoms between cases, thus there is a varying approach to treatment that is based on patient symptoms as well as individual reaction to treatments. Current treatment options are often used in combinations, examples provided in

Figure 1, and is augmented for each case individually. Considering there is no stable treatment option for patients, mediation of symptoms using a variety of pharmacological therapies until something works for that specific case is currently the only option, thus additional treatment options need to be explored.

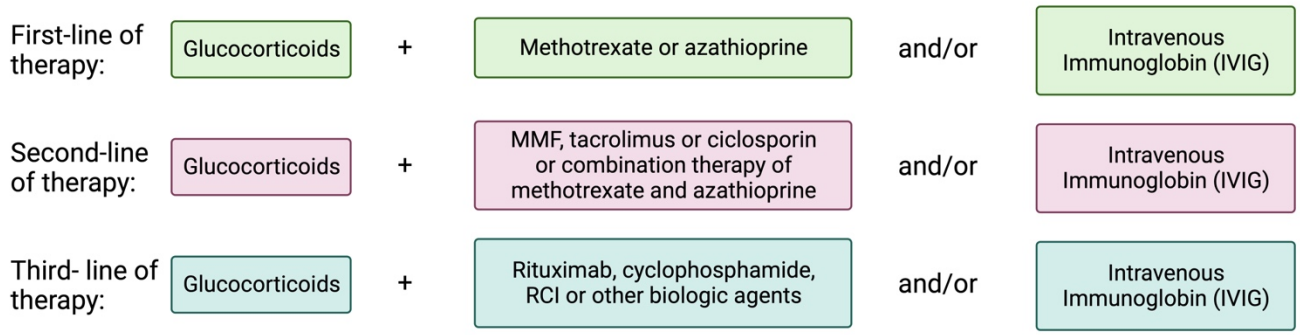

Figure 1. Potential pharmacological combination treatments for patients with IIM[15].

(Made with Biorender.)

Type of IIM	**MSAs associated with each IIM type.**
Dermatomyositis (DM)	anti-Mi-2, anti-MDA-5, anti-NXP-2, anti-TIF-1γ, anti-SAE-1/2 [16], anti-Jo-1, anti-ARS[17]
Polymyositis (PM)	anti-Jo-1, anti-ARS, anti- SRP, anti-(HMGCR)[17]
Immune-mediated necrotizing myopathy (IMNM)	anti- (HMGCR), anti-SRP[18]
Inclusion body myositis (IBM)	anti-cN1A, anti-Ro, anti-La[14]

Table 1. Myositis – specific autoantibodies (MSA) more predominantly found in each type of myositis.

2.1.3 *Autoimmunity and Myositis*

As outlined in the table above, there are myositis specific autoantibodies (MSA) expressed in myositis, but every antibody is developed through the immune systems recognition of its associating antigen. Thus, for every myositis autoantibody there is a relating autoantigen. Though this thesis is not focused on establishing the mechanism of autoimmunity in myositis (no cause is currently established), a basic understanding of potential theories of how this autoimmunity induces symptoms is vital background.

A potential autoimmune mechanism that results in myositis symptoms is that muscle damage is induced by cytotoxic (directed against foreign or self-antigens) T cells, this damage of muscle induces repair pathways that trigger an increase in autoantigen expression in muscle[19]. This T cell induced damage to the myocytes results in the release of intracellular autoantigens, free nucleic acids, and protein nucleic acid complexes to bind to Toll Like Receptors (TLRs; major inflammatory pathway mediators)[19]. These antigens experience post-translational modifications and can then acquire chemokine properties and activate autoreactive lymphocytes (B cells or T cells)[19]. This further drives the immune response and augments lymphocyte induced damage of regenerating muscle cells. Considering there is no known cause in patients currently, understanding the models that could aid mechanistic study designs is vital for future research.

2.1.4 *Models of Myositis*

There is a requirement for investigation into the human condition of myositis, and often in scientific literature animal models are valuable to help elucidate specific mechanisms or novel therapies before human treatment can commence. Particularly valuable animal models can relate as closely as possible to the human condition. A common model currently utilized in myositis literature is the experimental autoimmune myositis (EAM) rodent model. This model is induced

using purified myosin (foreign to the host animal) injected with an adjuvant (a substance that helps create a stronger immune response), and in many studies an exotoxin called pertussis toxin[7, 3 , 20]. Pertussis toxin (PT) is a bacterial toxin that in humans is known as *Bordetella pertussis,* which has been identified as a severe viral factor for its ability to promote bacterial colonization, modulate host immune responses, cause systemic effects and boost transmission[21]. In humans PT manifests as pneumonia, pulmonary hypertension, encephalopathy, and paroxysmal cough also known as whooping cough[21].

It is well established that in order to induce an immune response to an antigen, a co-administered microbial product (like Freund's Complete Adjuvant, containing heat-inactivated mycobacteria) is often used[22]. PT is a multi-subunit complex that functions using two major units, the B-unit binds to a receptor (MAC-1; macrophage-1 or any glycoconjugate receptor) on the immune cells surface, the A-subunit is then released into the cell and disrupts intracellular signaling by irreversibly binding G proteins[22]. PT has various impacts on the immune system that include preventing T cell apoptosis, augmenting specific antibody responses, as well as enhancing the production of a number of cytokines (IL-4, IL-5, IFN-γ)[22]. Interestingly, PT has shown to induce a systemic inflammatory response, resulting in exacerbated brain injury in hemorrhagic or ischemic stroke by enhancing leukocyte infiltration to the brain and destroying the blood brain barrier in mice[23]. However, some EAM models use PT in conjunction with an adjuvant even though it shows systemic inflammatory activation without myositis-specific autoantibodies raising concerns on the validity of the model's induction.

In literature that uses the EAM model, it is commonly induced with an adjuvant and PT as outlined above. Myositis in humans is an autoimmune condition which often presents myositis specific autoantibodies in order to mimic the autoimmunity of the human model. It is

safe to assume that a form of autoantibodies would be produced in the animal model as well. Allenbach et. al. 2009, evaluated anti-myosin antibodies and myositis specific autoantibodies in EAM animals that received PT, and found that a western blot demonstrated that EAM animals did produce antibodies against myosin proteins, but did not present any autoantibodies that are expressed in patients (shown via immunoassay dot blot)[7]. Interestingly, EAM models that were induced without PT were induced in *SJL/J* animals that have a gene mutation making them susceptible to autoimmune encephalomyelitis and there was no evaluation of autoantibody production on these EAM animals[24, 6, 25]. Given that myositis is an autoimmune disease, the animal models used to investigate this disease in the literature should mimic what is known about the human disease as closely as possible. Thus, in these EAM models that utilize PT, antibodies against myosin may not be sufficient to mimic the human condition.

2.2 Introduction to Mitochondrial Bioenergetics

2.2.1 Overview of Mitochondrial Bioenergetics

Mitochondria are double membrane-bound organelles of a cell with one of their major responsibilities being energy generation in the form of ATP (Adenosine Triphosphate). This energy generation is done by utilizing a series of enzymatic pathways that catabolize glucose and fatty acids that support oxidative phosphorylation that is mostly regulated by the electron transport chain. A by-product of oxidative phosphorylation is superoxide generation. Superoxide can be utilized as a signal within the cell to trigger additional cellular processes, but a build-up of superoxide can impact cellular function significantly. The balance between energy and superoxide generation within mitochondria is termed mitochondrial bioenergetics. Mitochondrial bioenergetics is regulated by balancing the ratio of energy demand to energy generated, or ADP to ATP homeostasis. Evaluation of cellular mitochondrial ability to regulate

ATP/ADP provides insight on metabolic impairments. When impairments to ATP/ADP homeostasis occurs, it can be termed mitochondrial dysfunction.

2.2.2 *Oxidative Phosphorylation*

The electron transport chain consists of four multimeric complexes and an ATP synthase termed complexes I-V, all located on the inner membrane space[26]. Complex I, NADH dehydrogenase, is a macromolecular complex consisting of iron-sulfur clusters (Fe-S), flavin mononucleotide (FMN) and a lipid-soluble electron mobile carrier (UQ) which is implanted in the lipid bilayer of the inner membrane of the mitochondria[26]. Complex I oxidizes NADH produced from the TCA/Kerbs cycle to NAD+, passing the electrons by reducing a series of Fe-S clusters from FMN to ubiquinone (UQ)[26]. Complex II, succinate dehydrogenase, which is a FAD-linked enzyme that donates the electron from succinate oxidation to fumarate (from the TCA cycle), to ubiquinone[27]. The electron from complex I oxidation of NADH, and the electron provided by complex II oxidation of $FADH_2$ is used to reduce ubiquinone (UQ) to ubiquinol (UQH_2)[28]. Ubiquinol (UQH_2) is then oxidized by complex III, which transfers electrons to the second mobile electron carrier cytochrome *c*. Cytochrome *c* is a heme protein that is oxidized by complex IV, also known as cytochrome *c* oxidase (COX)[27]. Complex IV then transfers electrons to oxygen, which then forms water utilizing two protons from the matrix. Complex V, or ATP synthase, is the driving force of ATP production by adding an inorganic phosphate group to existing ADP to create ATP (***Figure 2)***[27]. In order for this to occur an energy gradient is developed across these membranes.

During electron transfer through the complexes of the ETC, energy is released from the oxidation of reducing equivalents and is used to pump protons out of the mitochondrial matrix[27]. The complexes that assist in proton pumping are complexes I, III, and IV. This pumping of

protons results in a change in pH (ΔpH) as well as charge in the IMS and matrix. The IMS has a lower pH (higher concentration of H+) with a higher positive electrical charge, thus protons are pumped across the inner membrane against an electrical and chemical gradient, creating a proton motive force (PMF)[29]. PMF is based on the difference in electrical potential, also referred to as membrane potential ($\Delta\psi$) and the difference in pH (ΔpH)[29]. This energy gradient is utilized by ATP synthase and is generated when protons flow back into the matrix through ATP synthase, driving the phosphorylation of ADP to ATP[29]. When protons flow through a channel in the enzyme ATP synthase (complex V), a mechanical movement of the rotor portion of the protein spins, this provides the energy to add an inorganic phosphate group (P_i) to ADP to form ATP[27]. This uses the PMF to drive this reaction, and also lowers the membrane potential as protons are pumped into the matrix.

Oxidative phosphorylation (OXPHOS) is the cellular process that generates ATP, these complexes assist in ATP production. OXPHOS is regulated by cellular energy demand, the more available ADP and free P_i the more OXPHOS occurs. This thesis is interested in ADP sensitivity, which is impacted by phosphate shuttling. Thus, phosphate shuttling enzymes like mitochondrial creatine kinase (mtCK), outer mitochondrial membrane pore called the voltage dependent anion (VDAC), and adenine nucleotide translocase (ANT) assist in the regulation of OXPHOS and will be discussed further (2.2.4).

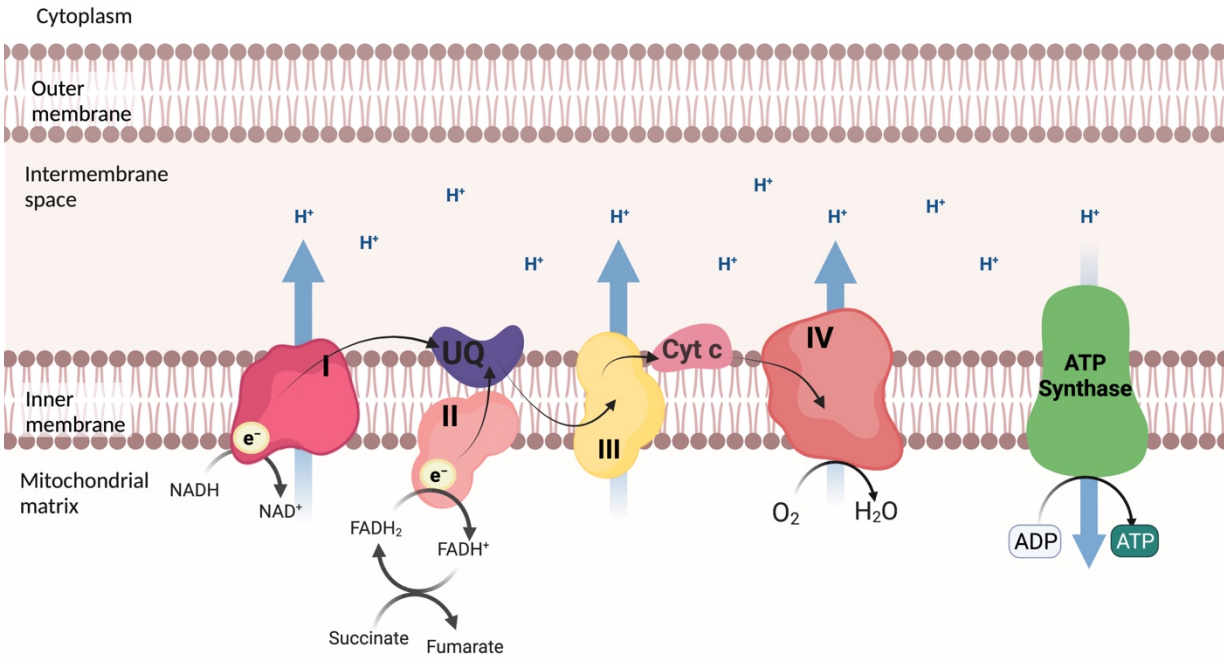

Figure 2. Visualization of key contributors to the ETC. The electron transport chain, with all complexes demonstrating the exchange of electrons and how they move through the ETC utilizing the membrane potential made from proton pumping, creating a water molecular and generating proton motive force to stimulate ATP synthase thus producing ATP. (Made with Biorender.)

2.2.3 *ROS formation*

As outlined above, the ETC is made up of five complexes that aid in ATP production. Of the five complexes three of these complexes pump protons against a chemical and electrical gradient that develops across the membranes of the mitochondria. Complexes I, III, and IV guide electrons through a series of redox (oxidation-reduction) reactions utilizing the free energy released to create a proton motive force that drives ATP synthesis by complex V[30]. Reactive oxygen species (ROS) are produced mainly as superoxide radical anions ($O_2^{\cdot -}$) and occurs when electrons leak or slip in unwanted side reactions from complexes or coenzymes of the ETC and onto molecular oxygen within the mitochondria[30]. When superoxide is generated, it is

transformed to the more stable hydrogen peroxide (H_2O_2) through the activity of matrix Mn-SOD or Cu,ZnSOD in the intermembrane space[31]. The compartmental localization of this enzyme demonstrates the importance of removing mitochondrial $O_2^{\cdot -}$. Complex I of the ETC releases $O_2^{\cdot -}/H_2O_2$ into the mitochondrial matrix, where complex III releases $O_2^{\cdot -}/H_2O_2$ into the cristae lumen and IMS[32]. Evidence evaluating knockout animals for Mn-SOD demonstrated prenatal fatality unless provided a SOD mimetic[31], demonstrating the cellular importance of Mn-SOD. Once superoxide is converted to H_2O_2 it is membrane-permeative and is also actively transported by aquaporins[31]. As H_2O_2 leaves the mitochondria and once in the cytosol it can be converted into H_2O by cytosolic antioxidant systems like glutathione peroxidase, and thioredoxin peroxidase[33]. ROS (or H_2O_2) is a naturally forming by-product of OXPHOS and, in stable physiological concentrations, is required for normal cell function but in excessive quantities can result in oxidative stress[33]. When ROS concentrations are in excess it can impact cellular functions and result in complications like cell death, inflammation, and growth arrest[32]. When H_2O_2 is in stable concentrations it is known to be a major physiological signaling agent assisting in cellular functions like proliferation, differentiation, and migration[32]. This concept of steady-state H_2O_2 being a vital signal utilized by the cell was termed oxidative eustress[32]. Thus, it is vital for proper cell function to carefully monitor superoxide production.

The evaluation of ROS production within this thesis is a vital piece of information that helps identify if the myositis phenotype seen in the EAM model is still prevalent in a model without PT. Meyer et. al. (2017), found that H_2O_2 production in the presences of glutamate and malate with saturating ADP concentrations in muscle fibers of dermatomyositis patients were sevenfold higher than that of control and non-dermatomyositis patients[3]. This group also evaluated ROS levels, by electron paramagnetic resonance, demonstrating significantly higher ROS levels in the

gastrocnemius and quadriceps of EAM mice than control animals[3]. This group concluded that there is a mitochondrial dysfunction present in both the EAM model and patient skeletal muscle[3]. Thus, this thesis is interested if a PT-free EAM model maintains this previously identified mitochondrial dysfunction.

2.2.4 *Phosphate shuttling systems*

Once ATP is made within the mitochondrial matrix it needs to exit the matrix in order to be used for cellular processes as energy. It travels into the IMS then from the IMS through the OM into the cytosol. It first goes from the matrix through a complex called adenine translocator (ANT) located in the IM[34]. From there it is able to exit the mitochondria using a voltage-dependent anion channel (VDAC) located on the outer membrane of the mitochondria, which allows metabolites through by forming an unspecific channel[34]. This process of shuttling ATP out of the mitochondria to where it is needed is the creatine independent process outlined in ***Figure 3*** below on the left.

There exists both cytosolic creatine kinase (CK) and mitochondrial CK (mtCK), which both are enzymes that catalyze the reversible reaction of phosphocreatine (PCr) and ADP to creatine (Cr) and ATP. These enzymes together are central controllers of cellular energy homeostasis, by building up rapidly diffusing PCr to assist with ATP demand[34]. This compartmentation of CK allows for the maintenance of high local ATP/ADP ratios in the vicinity of energy demand (for example contracting muscle cell), allowing for maximal ATP supply, and keeping the ATP/ADP ratio low within the mitochondrial matrix to stimulate OXPHOS[34]. VDAC permeability is regulated and can result in a rate-limiting diffusion barrier, which is detrimental to a high energy demand environment. PCr has a slightly faster diffusion rate compared to ATP allowing for faster localized ATP availability[34]. Thus, the Cr dependent shuttling system can provide an

efficient energy shuttle to bridge the gap between the site of energy generation and where the energy is required[34].

This thesis is interested in the activity of mtCK to determine how ADP sensitivity and phosphate shuttling is impacted in skeletal muscle in this EAM model. Without incorporating creatine within our experiments impairs our ability to evaluate how mtCK is impacted within this model, or if there is a compensation not recognized previously due to this creatine oversight.

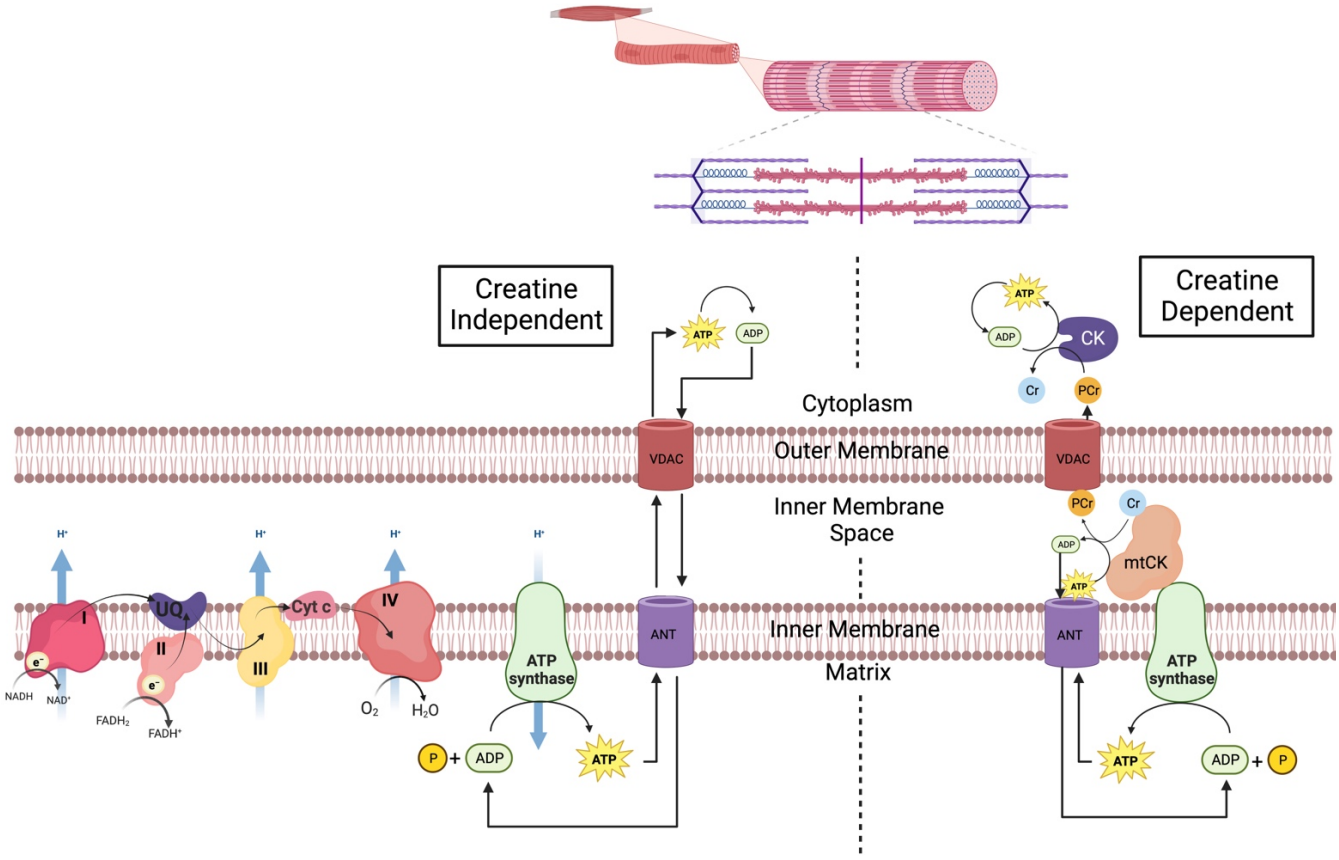

Figure 3. Creatine independent vs. creatine dependent phosphate shuttling. Demonstration of different ways a contracting muscle can receive ATP from the mitochondrial matrix. (Made with Biorender.)

2.3 Muscle Contraction

2.3.1 *Introduction to muscle contraction*

To understand the mechanism of muscle contraction it is vital to understand the structure of striated muscle. These muscles are comprised of many individual muscle fibers. Inside the muscle fibers there are units called myofibrils which are parallel thin and thick filaments. These filaments run longitudinally and are known as sarcomeres[35]. The thick filaments of myofibrils are made up of myosin protein that have a heavy chain and two pairs of light chains. These myosin filaments have two heads that have an actin-binding site that helps them attach to the thin filament[35]. The thin filaments are comprised of actin, tropomyosin, and troponin. Actin combines with another actin to form an intertwined double-stranded filament that is covered by tropomyosin[35]. Tropomyosin covers the active site on these actin myosin filaments while the muscle is inactive.

For muscle contraction to occur an action potential fires causing depolarization in the myocyte membrane. This depolarization is spread to the entire muscle fiber and causes confirmational changes to dihydropyridine receptors. This conformational change results in the opening of a ryanodine receptor on the sarcoplasmic reticulum which is a storage site for calcium[35]. When calcium is released it binds to troponin resulting in the shifting of tropomyosin, allowing myosin heads to attach to actin and form a cross-bridge[35]. This resulting cross bridge then cycles to shorten and relax sarcomeres. Addressed below, several aspects of this process are ATP-dependent and can be impacted by mitochondrial OXPHOS function (section 2.3.2).

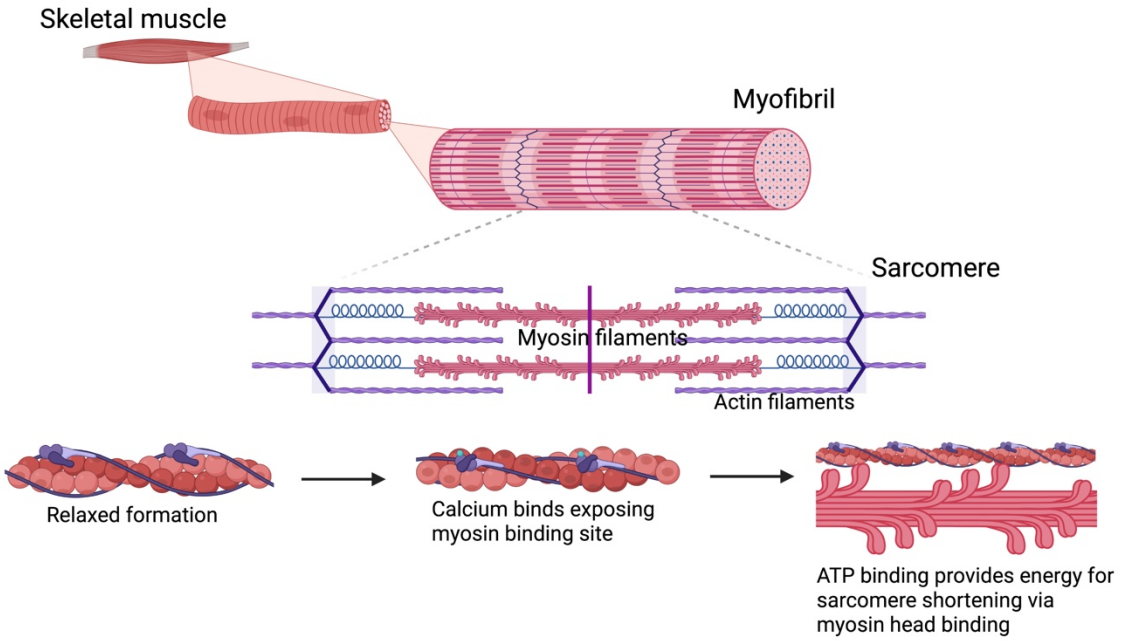

Figure 4. Visual representation of skeletal muscle structure and muscle contraction. (Made with Biorender.)

2.3.2 *Relationship between Mitochondrial ATP synthesis and Contraction*

A skeletal muscle cells main function is to convert biological energy into mechanical force, which is critical for movement. During continuous muscle contraction the process of cellular energy transduction is largely mediated by the mitochondria and the force-generating capacity of the myofibrils[36]. As outlined above, mitochondria generate ATP through OXPHOS and this ATP (as well as other contributors like sodium and potassium, and SERCA which is not explored here for simplicity) is used by the myofibrillar ATPase to generate force during contraction[36]. Mitochondrial ATP production is important for muscle function, which is demonstrated by the volume of mitochondria within human skeletal muscle commonly being 3-8% with this volume being impacted based on muscle activity levels[36, 37]. Some muscle cells have higher mitochondrial content contributing to their higher oxidative capacity [36], thus maintaining skeletal

muscle contraction will partially depend on the regulation of mitochondrial oxidative phosphorylation matching the demand for ATP.

To understand how muscle fibers utilize ATP to produce force we must first understand the structure and formation of the myosin – actin cross-bridge outlined above and in ***Figure 4***. This cross-bridge cannot form until an action potential is fired and calcium is released saturating the sarcomere and binding to troponin to move tropomyosin exposing the myosin binding site on actin filaments. Myosin heads then go through a confirmational change and bind to actin forming said cross-bridge. Cross-bridge cycling occurs when ATP binds to an ATP-binding site on the myosin head, and myosin disconnects from actin breaking the cross-bridge[35]. ATP is then broken down to ADP and P_i, which causes the myosin head to twist and move toward the end of the actin filament[35]. The P_i is released and the ADP bound myosin binds to a new location on the actin. Releasing ADP myosin returns to its original configuration resulting in a pull of the actin filament causing the shortening of the sarcomere or the muscle to contract[35]. This cross-bridge cycling continues until the calcium levels stabilize to return tropomyosin to its original location of covering the myosin binding sites on actin filaments, returning the muscle to its relaxed state[35].

ATP demand increases significantly during the transition from rest to contraction, and the longer the muscle is required to contract as well as the intensity to which it needs to contract impacts ATP production. To support this increasing energy demand during sustained contraction, skeletal muscle utilizes anaerobic metabolism, which is the process that includes phosphocreatine pathways and muscle glycogen breakdown[38, 39]. The muscle also uses oxygen to produce ATP by OXPHOS, but this is limited by oxygen delivery to the muscle[38]. The production of ATP using OXPHOS by using reducing equivalents from carbohydrate and fat

metabolism within the mitochondria, is called aerobic metabolism[39]. When the muscle is experiencing sustained contraction, it must utilize multiple modes of ATP synthesis in order to satisfy the ATP demand.

2.3.3 *Relationship between Mitochondrial ROS synthesis and Contraction*

It is commonly thought that an increase of ROS is generation due to the increased oxygen consumption that occurs with the increase in mitochondrial activity during exercise. Although, when basic principles of bioenergetics are considered, it is understood that proton pumping cannot occur without electron flux to oxygen, and electron flux cannot occur without proton pumping[40]. Without complex V pumping protons back into the matrix, membrane potential increases, proton pumping and thus electron flux would slow[40]. With membrane potential increased and limited proton pumping or electron flux, the rate of electron slip increases resulting in superoxide generation at complexes I and III that is almost immediately dismutated to H_2O_2 by superoxide dismutase (Mn-SOD, Cu,ZnSOD)[40, 29]. Thus, when there is an increase of ATP demand reflected by a decrease in the ATP/ADP ratio, membrane potential is lowered by pumping protons back into the matrix by complex V to produce ATP and lowering the rate of superoxide production[40]. In the context of sustained muscle contraction, there is an increase in energy demand, which increases the concentration of ADP and drives OXPHOS to produce ATP. This theory is evident during *in vitro* assays given the addition of ADP to assay media attenuates H_2O_2 emissions when supported by NADH (complex I) or $FADH_2$ (complex II) generating substrates[40]. In the context of disease models, the evaluation of how ADP is able to attenuate H_2O_2 emissions in experimental groups provides insight on potential mitochondrial dysfunctions that could impact contractile abilities. Although there are other sources of superoxide generation than the ETC within the mitochondria, including NOX4, dehydrogenases

like pyruvate dehydrogenase, monoamine oxidases, and enzymes of the TCA cycle which are examples of other sources of superoxide that dismutates into H_2O_2[40, 41]. Moderate levels of superoxide generation are required for normal cell function as H_2O_2-mediated pathways are activated in response to exercise and mediate adaptations like mitochondrial biogenesis and increasing antioxidant production. While these sources of superoxide are expressed in muscle a lot still needs to be characterized of the effect of exercise on H_2O_2-generating pathways.

Mitochondria are not the only sources of H_2O_2 within skeletal muscle, another major source of H_2O_2 within skeletal muscle during exercise is nicotinamide adenine dinucleotide phosphate (NADPH) oxidases (NOX) located on the sarcoplasmic reticulum, transverse tubules, and sarcolemma[42]. Although NOX is thought to be a major contributor of superoxide generation within skeletal muscle, this thesis is focused on mitochondrial H_2O_2 production and is concentrated on literature that demonstrates the relationship that mitochondrial H_2O_2 has with contraction. Although, it should be noted that reactive nitrogen species (RNS) or reactive oxygen-nitrogen species (RONS) also increase during contraction, but is not reviewed due to the nature of this thesis[40].

2.3.4 *Relationship between Inflammation and Contraction*

The immune system plays a vital role defending an organism against disease or infection, with the use of inflammation it is able to signal and attack potential pathogens, release substances to assist in the healing process, and kill injured or infected tissues to reduce damage or spread. However, in chronic conditions (like autoimmune diseases) this inflammatory response leads to significant damage to cells. Muscle atrophy occurs when there is more protein degradation occurring than protein synthesis, which leads to the loss of myofibrillar proteins, reducing fiber cross-sectional area, and impairing contractile ability. Muscle protein degradation

systems are modulated by a network of signaling pathways activated or suppressed by hormones and cytokines[43]. Loss of muscle is often associated with proinflammatory cytokines like TNF-α, IL-1β, IL-6, and IFN-γ[43].

Chronic inflammatory conditions like autoimmune conditions upregulate cytokine production and thus impact muscle function. TNF-α plays a critical role in inflammation, apoptosis, and immune system development, where in skeletal muscle it influences satellite cell proliferation[44]. TNF- α is secreted from myotubes inhibiting regeneration by inhibiting Notch-1 in satellite cells and C2C12 myoblasts, this inhibition to Notch-1 is done so by transcriptional repression[45]. IFN-γ is known to influence skeletal muscle homeostasis and repair, but in high doses is able to impact myogenesis[44]. IFN- γ expression is increased in *mdx* animals at 4wks and 12wks, and demonstrates decreased proliferation in these animals[46], but in the absences of IFN- γ an improvement in muscle function was seen in *mdx* mice[46]. IL-6 is a cytokine that has both pro and anti-inflammatory effects depending on the immune cell environment[47]. Chronic inflammation impacts the liver and thus impacts muscle growth, by the overexpression of IL-6 which causes the liver to become resistant to GH (growth hormone) resulting in a decrease in IGF-1 (insulin-like growth factor -1) production and thus directly impacting muscle growth[48]. Cytokines like IL-6, TNF- α are upregulated in myositis and can thus, impact skeletal muscle contraction by limiting muscle cell proliferation with the presence/chronic expression of specific proinflammatory cytokines resulting in muscle breakdown and decreasing myofibril force production capacity.

2.4 Relationship Between Inflammation and Skeletal Muscle Mitochondria

Understanding the importance of the mitochondria for skeletal muscle health, and the importance of the immune systems use of inflammation for cellular health. The focus shifts to

elucidate the relationship between skeletal muscle mitochondria and inflammation. Mitochondria are emerging as modulators of inflammation, damaged or dysfunctional mitochondria release signals known as mitochondrial-derived damage-associated molecular patterns (mito-DAMPs)[49]. These signals are recognized by specific pathways of the innate immunity like pathogen-associated molecular patterns (PAMPs) [50]. When damage occurs to skeletal muscle their mitochondria assist in the activation of an acute inflammatory response that is necessary to stimulate myofibril regeneration. Although exhaustive signaling associated with dysfunctional mitochondria can be detrimental to muscle health. This mitochondrial dysfunction resulting in excess mito-DAMP release exacerbates the inflammatory response and impacts muscle homeostasis[49].

There are many mito-DAMPs released that enhance inflammatory processes. Each mito-DAMP are recognized by specific pathways in the innate immune system, and result in an increase in pro-inflammatory responses. Specifically, superoxide has been shown to activate inflammasome signaling by activation of NLRP3 inflammasome, which was identified through the inhibition of autophagy and mitophagy resulting in an increase of superoxide generation that activated NLRP3 inflammasome[51]. But, when rotenone or antimycin (complex I inhibitors) was used to increase mitochondrial superoxide production in NLRP3 knockdown cells, this resulted in the decrease of an NLRP3 activated cytokine IL-1β (interleukin 1- β; pro-inflammatory cytokine) demonstrating the requirement of superoxide activation to trigger cytokine production[51].

The activation of mito-DAMPs due to muscle injury results in specific cytokine activation, like interleukin – 6 (IL-6), interleukin – 1β (IL-1β), and monocyte chemoattractant protein 1 (MCP-1)[52]. When injury to skeletal muscle occurs the damaged myofibers release MCP-1,

which activates satellite cells by attracting monocytes to site of damage[49], excessive amounts of MCP-1 can be pathogenic and is found across many chronic inflammatory disorders including all types of IIM[53]. There are innate immune cells that reside in tissue to help promote an immune response at the site of injury, some of these cells are tissue-resident macrophages. These macrophages can release cytokines and chemokines to trigger an immune response and some of these being the above-mentioned IL-6, and IL-1β. IL-6 signalling through the JAK/STAT pathway is known to promote muscle hypertrophy and regeneration, but chronic activation of STAT3 by IL-6 accelerates muscle breakdown[54]. To determine the impact of prolonged STAT3 activation, *mdx* mice were provided a STAT3 inhibitor and exhibited improved tissue repair demonstrated by an increase in myoblasts as well as myofiber cross-sectional area[54].

Interestingly, some of these pro-inflammatory cytokines can also impact mitochondrial function. TNF- α decreases membrane potential, which was evaluated in cells treated with TNF-α which demonstrated a dose dependent decrease in membrane potential caused by caspase 8 activation[55]. TNF-α was also shown to decrease mitochondrial function in cells treated with TNF-α demonstrated by basal respiration being decreased[55]. Similarly, IL-6 has been shown to regulate protein expression of mitochondrial fission proteins (Fis-1, DRP-1)[56]. Since an increase in mitochondrial fission (a process that segments parts of damaged mitochondria) by DRP-1 can trigger an increase in mitophagy[57], excessive elevation of IL-6 stimulating DRP-1 overexpression would hinder the mitochondrial environment. IL-1β is activated after injury and when in excess has been linked to decreased mitochondrial stability, releasing mitochondrial content to the cytosol, and impacting autophagy[58]. There is a clear relationship between mitochondrial dysfunction and inflammatory activation, which would be exacerbated in a

condition that experiences both autoimmune activation, mitochondrial dysfunction, and muscle injury, making inflammation and mitochondrial health an important focus for this thesis.

CHAPTER 3: RATIONALE AND HYPOTHESIS

3.1 Rationale

Myositis is a rare autoimmune condition that commonly results in chronic inflammation that impacts skeletal muscle by inducing proximal muscle weakness over time. Considering the limited understanding regarding this condition or its causes, the manner in which myositis develops over time and the extent of muscle weakness is unclear. Research in the EAM model has outlined how the number of injections impacts immune cell infiltrating into skeletal muscle by histology[7]. To date no studies have established a Pertussis Toxin (PT)-free model in a wildtype animal. Thus, the evaluation of a PT-free model of EAM induced in a WT animal, and its comparisons to the human myositis phenotype is informative for the literature to fully outline if this is a sufficient model to assess myositis.

The ability of a muscle to contract depends in part on the rate of ADP recycling into ATP and the disbursement of ATP throughout the cell. Skeletal muscle health is indicated by the ability of its mitochondria to regulate an energy equilibrium. There needs to be more investigation into the respiration capacity of skeletal muscle mitochondria in EAM animal tissues. However, previous literature has identified a mitochondrial dysfunction, measured as an increase in mitochondrial hydrogen peroxide emissions (mH_2O_2) and decrease in mitochondrial respiration, in skeletal muscle of myositis patients' biopsies and ROS production in EAM tissue[3]. With this increase in superoxide generation, as well as proximal muscle weakness, it is recognized that there is a decline in skeletal muscle health in myositis and thus within this EAM model. There is limited evidence outlining muscle or mitochondrial function in the EAM model.

An experimental autoimmune myositis (EAM) rodent model was employed for this thesis for multiple reasons. This model was augmented for our laboratory given animal ethics

restrictions, removing pertussis toxin was a requirement due to the additive effects when paired with the adjuvant. To induce this model, in-lab partially purified rabbit myosin was emulsified with two different adjuvants, which were purchased. Secondly, previous literature identified a mitochondrial dysfunction within the skeletal muscle of this model which justifies it's use for examining more specific relationships between mitochondria and muscle dysfunction[3]. Finally, considering the myositis animal models available, this model was the most plausible given the resources and training requirements.

3.2 Specific Objectives

The specific aims of this project were:

(1) To determine if repeated myosin and adjuvant injections in the absence of pertussis toxin decreases force production in diaphragm and tibialis anterior in a time-dependent manner, and if weakness occurs concurrent with or independent of atrophy.

(2) To determine if repeated myosin and adjuvant injections alter mitochondrial respiration or H_2O_2 emissions in a muscle-specific manner at Phase 2, in our PT-free EAM model.

3.3 Hypothesis

The specific hypotheses of this project were:

(1) Force production in the diaphragm and tibialis anterior will decrease in a time-dependent manner, with weakness occurring concurrent to atrophy.

(2) Repeated injections will result in a worsening phenotype, exacerbating mitochondrial stress responses in the modified PT-free EAM model.

3.4 Author Contributions

The majority of the experiments of this project were carried about by Madison Garibotti (MG) and Arshdeep Thuhan (AT). MG and AT performed all pilot studies, purified the myosin,

performed all injections, monitored all animals, collected anthropometric and lesion scores until sacrifice. Luca Delfinis (LD) performed all *in situ* and *in vitro* force production experiments, but analyses were performed by MG. MG harvested and prepared all tissues for respiration, and mH_2O_2 emissions. Due to the nature of all the fresh muscle experiments multiple people are required to conduct these experiments at the same time. Thus, MG completed either respiration or mH_2O_2 emission assessments, while AT completed respiration or Shahrzad Khajehzadehshoushtar (SK) completed mH_2O_2 emission.

3.5 Additional Contributions

The following work represents additional contributions made throughout my MSc that are not included in my thesis.

Co-Author Published:

Garibotti M.C., and Perry C.G.R.. (2023). Strength athletes and mitochondria: it's about 'time'. *The Journal of Physiology.* DOI: 10.1113/JP284856. Invited perspective.

Bellissimo C.A., **Garibotti M.C**., Perry C.G.R. (2022). Mitochondrial Stress Responses in Duchenne muscular dystrophy: Metabolic Dysfunction or Adaptive Reprogramming?. *Am J Physiol. Cell Physiol*. Sept 1 2022, 323(3): C718-C73010.1152/ajpcell.00249.2022. *Invited Review.*

Delfinis L.J., Bellissimo C.A., Gandhi S., DiBenedetto S.N., **Garibotti M.C.**, Thuhan A.K., Tsitkanou S., Rosa-Caldwell M.E., Rahman F.A., Cheng A.J., Wiggs M.P., Schlattner U., Quadrilatero J., Greene N.P., Perry C.G.R. Muscle weakness precedes atrophy during cancer cachexia and is linked to muscle-specific mitochondrial stress. *JCI Insight*. 2022 Dec 22; 7(24):e155147. Editor's Pick: https://insight.jci.org/this-month/2023/1

Bellissimo C.A., Gandhi S., Castellani L.N., Murugathasan M., Delfinis L.J., Thuhan A.K., **Garibotti M.C.,** Seo Y., Rebalka I.A., Sweeny G., Hawke T.J., Abdul-Sater A.A., Perry C.G.R. (2023) Adiponectin receptor agonism attenuates fibrosis, inflammation and mitochondrial H_2O_2 emission in diaphragm from the D2.*mdx* mouse model of Duchenne muscular dystrophy. In review, *FASEB J*. doi: https://doi.org/10.1101/2023.05.22.541826

Co-Author in Progress:

Thuhan A.K., **Garibotti M.C**., Delfinis L.J., Khajehzadehshoushtar S., Abdul-Sater A.A., and Perry C.G.R. 2023. Elucidating the role of macrophage reactive oxygen species production in a time course model of experimental autoimmune myositis (EAM).

Delfinis L.J., Gandhi S., **Garibotti M.C**., Thuhan A.K., Reid R.A., Khajehzadehshoushtar S., Ogilvie L.M., Matuszewska K., Periera M., Cheng A.J., Simpson J.A., Petrik J. and Perry C.G.R. 2021. Muscle mitochondrial pyruvate oxidation is reduced in early-stage ovarian cancer but partially restored in advanced-stage.

Gandhi S., Delfinis L.J., **Garibotti M.C**., Bellissimo C.A., Castellani L. N., Yakubov S., Edgett B.A., Backx P.J., Simpson J.A., and Perry C.G.R. 2021. Adiponectin-receptor agonism mitigates chamber-specific cardiac fibrosis and mitochondrial stress in the D2.*mdx* muscular dystrophy mouse.

Gandhi S., **Garibotti M.C**., Goli A., Miner S, and Perry C. G. R. 2024. The effects of coronary artery bypass grafts (CABG) on mitochondrial stress in human right atrial appendage.

CHAPTER 4: MATERIALS AND METHODS

Animal care

Female *BALB/c* mice were purchased from Envigo strain *BALB/cAnNHsd*, at an age range of 10 weeks to 16 weeks of age, which was chosen to control for sacrifice age across all time points and based on previous published literature[3,6,7,59] Upon arrival at York University's Animal Facility, these animals were housed and given at least 72 hours to acclimatize to the facility before treatments began. All mice were provided constant access to standard mouse chow and water ad libitum. Animals were monitored daily during treatment periods for general well-being, lesion development, and weight loss. If mice demonstrated signs of distress, treatment of that animal ceased, and the animals were sacrificed as soon as possible. Nine occurrences led to the replacement of new animals to maintain the sample size. All experiments and procedures were approved by the Animal Care Committee at York University following the approved protocol AUP 2019-17 in accordance with the Canadian Council on Animal Care.

Induction of EAM

Myosin protein was purified in-lab from rabbit skeletal muscle and stored in 50% glycerol, protocol provided by Dr. Leslie Leinwand (Appendix A). Freshly sacrificed rabbits were obtained by a commercial food supplier (Abate packers, Arthur, ON) which meets Canadian Health requirements of ethical treatment of animals, hindlimb and forelimb skeletal muscle tissue was used for purification. The purity of the myosin was verified using a western blot with a gradient gel (4-12%) with a Coomassie Blue in-gel total protein stain (Supplemental Figure 1). Visible bands were verified to correspond to myosin heavy and light chain as well as trace sarcomere proteins as published previously[60]. For the first treatment, this myosin was emulsified with an equal amount of Freund's Complete adjuvant (CFA, Sigma) containing

1mg/mL Mycobacterium tuberculosis to enhance the immune response to the myosin antigen. For all remaining treatments, the same myosin was emulsified with Freund's Incomplete adjuvant (IFA, Sigma). All treatments were 7 days apart, with 78.5 μL of the emulsified treatment injected subcutaneously on the back in four different sites (total volume animal received 314 uL, an injection at each shoulder blade, and one at either flank). This volume was calculated based on work done by Suzuki et al., 2005 whereby rabbit skeletal muscle-derived myosin was injected at a concentration of 3.3 mg/ml at 400 uL, equally split into four different locations on the animal. This approach was modified to inject 78.5 uL per location given we achieved a high myosin concentration of 4.303 mg/ml.

Experimental groups and phases

- Mice were randomly assigned to three groups as follows: Myosin treatment group: Receiving 50% purified myosin glycerol solution emulsified with 50% CFA for the first treatment, or 50% IFA for the remaining treatments.
- Glycerol/saline emulsified with CFA/IFA control group: Receiving 50% glycerol saline solution emulsified with 50% CFA for the first treatment, or 50% IFA for all remaining treatments.
- Glycerol saline control group: Receiving 75% saline to 25% glycerol.

The study was structured into distinct phases to capture the time-dependent effects of myosin and adjuvant injections. All 3 groups described above were assessed at each time point (see *Figure 5*). For Phase 1, animals received 3 injections over 14 days and were sacrificed 7 days after their final injection (Day 21). Tibialis and diaphragm force were evaluated, and animal tissues were removed under isoflurane anesthesia prior to euthanasia. All tissues were weighed, snap-frozen in liquid nitrogen and stored at -80°C.

For Phase 2, animals received 4 injections over 21 days to create a stronger phenotype than Phase 1 and were sacrificed 7 days after their final injection (Day 28). Tibialis and diaphragm force were evaluated, with the non-contracted tibialis anterior and diaphragm muscles placed in BIOPS buffer (see below) to be utilized for mitochondrial bioenergetic measures. All other tissues were weighed and snap-frozen in liquid nitrogen and stored at -80°C.

For Phase 3, animals received 4 injections over 21 days and sacrificed 28 days after their final injection to determine if any prior effects of inoculations were reversed. All tissues were weighed and snap-frozen in liquid nitrogen and stored at -80°C.

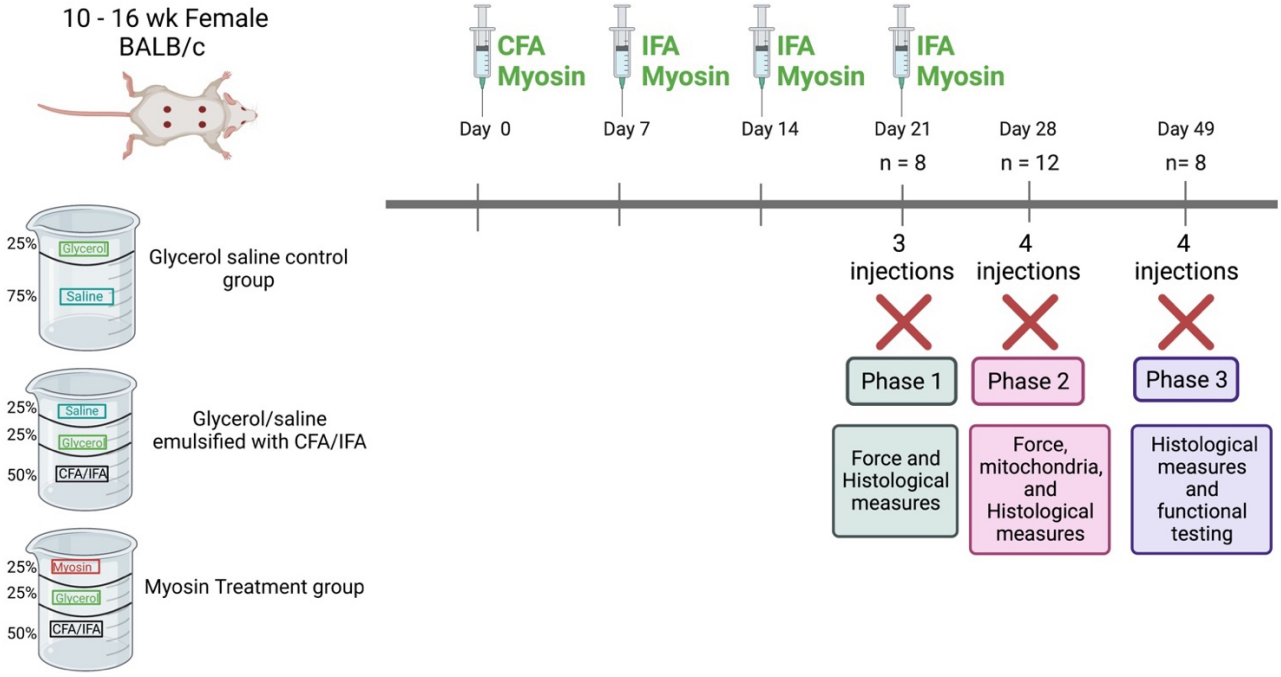

Figure 5. Outline of experimental treatments, dosing regimen and sample collections (Made with Biorender).

Forelimb Grip Strength

Grip strength was assessed as published previously[61]. Specifically, a metal grid was attached to a force transducer, set to peak tension setting. Force transducer was placed on a tabletop, with the metal grid hanging off the edge of the table (allowing enough space for the

metal grid to swing when the mice grab onto it without hitting the table). Mice were removed from their cages and held by their tails, placed just in reach of the metal grid, allow the mice to grab with only their forelimbs. Keeping tension on the tail of the mouse, the mouse was pulled away from the grid until their grasp was broken and they let go. The value produced by the force transducer was then collected, and the mouse was returned to their cage. This was repeated for the same mouse twice more, allowing for a minimum rest of 30 seconds between each assessment. If force was not produced, grip strength was not recorded. Grip strength assessments was completed at endpoint for each phase.

Cage Hangtime

Protocol adapted from previous literature to conduct voluntary muscle assessments[61]. A mouse was placed on a cage lid, which was inverted approximately 35 cm over a empty cage. Once the cage was inverted a manual timer was used to record the time that the mouse could hold onto the cage lid. This process allows for 3 attempts with 30 second breaks between each attempt, or until the mouse could stay in the inverted state for 3 minutes without dropping. Cage hangtime assessments were completed at endpoint for each phase.

In situ Tibialis Anterior Force and In Vitro Diaphragm Force

Force protocols described below have been adapted from previous literature[62]. For *in situ* tibialis anterior force, mice were anesthetized with 3-4% isoflurane then placed on a heating pad. The muscles on the front of the lower leg were exposed, allowing for the tendons that connect at the top of the foot to be exposed as well. The tibialis anterior tendon was identified but not severed. A suture was secured around the base of the tendon allowing for the suture to form a large loop. The tendon was then severed, and the muscle was then carefully isolated from the other muscles. The suture was then attached to the Aurora Scientific 305C muscle lever arm with a hook. The

knee was secured with a vertical knee clamp immobilizing the knee joint with a 27G needle. Contraction of the tibialis anterior was controlled through the stimulation of nerves of the lower hindlimb specifically the peroneal nerve this was done by placing the probes in the small gaps of fascia in between muscles. The stimulating probes are not placed directly into the tissue of interest to prevent damaging the tissue while inducing contraction. Optimal length was determined at varying lengths by using 1Hz twitches separated by a minimum of 30 seconds to minimize twitch potentiation. Once optimal length was determined, force as a function of stimulation frequency was measured during 11 isometric contractions at varying stimulating frequencies (1, 10, 20, 30, 40, 50, 60, 80, 100, 120, 200 Hz). The muscle was then weighed, and flash frozen with liquid nitrogen.

To collect *in vitro* diaphragm force, the muscle was removed from the mouse and placed into a petri dish with ringer's buffer. The diaphragm was then cut into strips from the central region of the lateral costal hemidiaphragm. A suture was then tied to the central tendon as well as the ribs, this was then transferred into an oxygenated bath filled with oxygenated ringer's solution. The diaphragm was attached to the lever arm at the central tendon, while the suture loop secured to ribs was attached to force transducer. The diaphragm strip was then situated between two platinum electrodes. Optimal length was then determined using twitches at varying muscle length. Length was determined based on highest force output per twitch. Once optimal length was determined force as a function of stimulation frequency was measured during 10 isometric contractions at varying stimulating frequencies (1, 10, 20, 40, 60, 80, 100, 120, 140, 200 Hz). Force production was normalized to cross-sectional area of the muscle strip considering only a section of the diaphragm was contracted. Cross-sectional area was determined using histological analysis explained below.

Histological analysis and Immunohistochemistry

Tibialis anterior (TA), diaphragm, extensor digitorum longus (EDL), quadriceps, and plantaris muscles were embedded into O.C.T. medium, cut into 8-um-thick sections with the cryostat, maintaining a constant temperature of -20°C. To assess damage, a Hematoxylin and Eosin staining procedure was utilized. Hematoxylin stains DNA content (nuclei), eosin stains plasma membrane and cytoplasm. All slides were air dried for 5-10 minutes before hematoxylin was added to all sections for minimum 30 seconds. Slides were rinsed gently with warm tap water and blotted dry before eosin was added for 5 minutes. These sections were then dehydrated with a range of ethanol rinses starting at 70% ethanol to 99% ethanol on the last rinse. To seal the sections onto the slides, the sections were rinsed in xylene and a mounting medium was placed on top of the slide to secure the cover slip in place. Once dried for 24 hours images of the sections were taken on the EVOS imaging microscope and analyzed accordingly. To assess immune system infiltration into muscle for this model, the precent of immune cell infiltration was assessed utilizing ImageJ software by comparing the area of the entire image to the area of immune cell infiltrates.

To allow for the assessment of muscle fiber type-specific atrophy within these samples, the muscle tissue was embedded and cut as previously explained and stained with myosin heavy chain-specific antibodies. These antibodies bind to different myosin isoforms, allowing for the muscle fibers to fluoresce different colours for identification during analysis. Slides were air-dried for 5-10 minutes then blocked with goat serum in PBS for an hour at room temperature. All primary antibodies were purchased from the Developmental Studies Hybridoma Bank (University of Iowa), and secondary fluorescent antibodies (goat anti-mouse) were purchased from Invitrogen, Thermo Fisher Scientific (Burlington, ON, Canada). Slides were incubated

with primary antibodies against myosin heavy chain MHCI (BA-F8 at 1:25 dilution, igG2b), MHCIIA (SC-71 at 1:500 dilution, igG1), and MHCIIB (BF-F3 at 1:50 dilution, igM) for 2 hours whereas MHCIIx did not receive a primary or secondary antibody and are thus represented as all black fibers. These slides are washed with PBS then incubated with secondary (MHC I; Alexa Fluor 350 IgG2b; 1:1000) (MHC IIa; Alexa Fluor 488 IgG1; 1:1000) (MHC IIb; Alexa Fluor 568 IgM; 1:1000) antibodies for an hour. These slides are once again washed 3 times in PBS for 5 minutes and mounted with ProLong antifade reagent. Slides can then be imaged by the EVOS imager, and cross-sectional area analyzed to determine fiber-type specific atrophy within the muscle samples.

Western Blot/Coomassie Gel

Protein concentrations of the purified rabbit myosin was determined using a Bradford assay (ThermoFisher, Cat# 23236). 0.5-1 μg/μL of denatured and reduced protein was subjected to 4-12% gradient polyacrylamide gel. This gel was than fixed using an isopropanol fixing solution (25% isopropanol, 10% acetic acid, 65% H_2O) and rotated at room temperature for 60 minutes. The gel was then covered in rapid Coomassie blue staining solution (10% acetic acid, 0.006% Coomassie Brilliant Blue G-250 BioRad, 90% H_2O) and rotated gently overnight at room temperature. Gel was then covered in 10% acetic acid to destain and shook at room temperature for 2 hours. A photograph of the gel was taken using an iPhone, gel was not used for quantification but to validate purity.

Mitochondrial Bioenergetic Assessments

Preparation of permeabilized muscle fibers

The assessment of mitochondrial bioenergetics was performed by removing the tibialis anterior and the diaphragm and placing them in BIOPS on ice. From there, under a microscope,

all tendons, connective tissue, and fat was removed from the muscles followed by partial separation of fibres along the longitudinal axis into small bundles (2.1 – 5.1 mg for TA and 0.8-2.0 mg for diaphragm). These bundles were blotted to remove excess buffer and weighted in tared cold 1.5 mL of BIOPS, these weights were utilized for analysis since during the respiration assay small pieces of bundles can detach. The bundles were then treated with 40µg/mL of saponin in BIOPS buffer. These bundles were rotated for 30 minutes at 4°C. From there the bundles were rotated for 15 minutes in buffer Z at 4°C to remove saponin and the cytoplasm. The permeabilized muscle fiber bundles (PmFB) that were utilized for Complex I-supported mH_2O_2 emissions is treated with 0.035µg/mL of CDNB to deplete endogenous glutathione in BIOPS buffer instead of saponin.

Mitochondrial Respiration

High-resolution O_2 measurements were conducted in 2 mL of respiration medium, either buffer Z or 20mM Creatine buffer Z, using the Oroboros Oxygraph-2k with continuous stirring at 750 rpm and temperature control at 37 °C. Buffer Z containing 20 mM Creatine was utilized to saturate mitochondrial creatine kinase (mtCK) promoting ADP transport by improved phosphate shuttling, buffer Z without creatine prevents the activation of mtCK[62,63]. To evaluate ADP-stimulated respiratory kinetics, procedures to stimulate complexes I and II-supported mitochondrial respiration were utilized. 5 mM pyruvate and 2 mM malate were added as complex I-specific substrates (considering its generation of NADH to saturate electron entry into complex I) followed by a titration of sub-maximal ADP (25, 100, 300, and 500 µM) and maximal ADP (5 mM and 7mM) [62]. 10 mM of glutamate was added after ADP saturation, cytochrome *c* was then added to test for mitochondrial membrane integrity[62,63]. The last substrate in the pyruvate malate protocol was 20 mM succinate, this saturates the electron entry

into Complex II. To evaluate the respiratory capacity when provided substrates to promote fat oxidation, 5 mM of L-Carnitine, 0.02 mM of Palmitoyl-CoA, and 0.5 mM of malate was added into the chambers, which contain solely buffer Z containing 20mM creatine. The above-mentioned ADP, cytochrome *c*, and succinate titrations are all kept the same, but this protocol does not include glutamate considering it is a glycolytic substrate.

All experiments were conducted with 5 μM blebbistatin added in the respiratory medium to prevent bundle contraction, which has been shown to occur in previous publications[63]. Polarographic oxygen measurements were acquired in 2 second intervals with the rate of respiration derived from 40 data points and expressed as pmol/s/mg wet weight.

Mitochondrial H_2O_2 Emissions (mH_2O_2)

mH_2O_2 was determined by spectrofluorometry in a cuvette with continuous stirring at 37 °C, in 1 mL of Buffer Z with 10 μM Amplex Ultra Red (AUR), 1 U/mL horseradish peroxidase. State II mH_2O_2 (maximal emission in the absence of ADP) was induced using the Complex I-supporting substrates (NADH) pyruvate (10mM) and malate (2 mM) to assess maximal mH_2O_2 without ADP present. Following the induction of state II mH_2O_2, a series of ADP titrations are employed (25, 100, 500 μM) to evaluate the mH_2O_2 emissions that occur during oxidative phosphorylation[62]. After the experiment the PmFB are placed in the freeze-dryer overnight and were weighed on a microbalance. The rate of mH_2O_2 emissions was calculated from the slope using a standard curve established with the same reaction conditions and normalized to fiber bundle dry weight[62]. This same protocol was repeated to evaluate succinate driven mH_2O_2, with 10 mM of succinate added into either creatine AUR or no creatine AUR (to identify if there was a change in mH_2O_2 when mtCK is activated), this was then followed by the same ADP titrations.

Lesion Score Assessments

During the treatment period, recognition of lesion development at the injection site was made and monitored. To assist in understanding animal welfare lesions were monitored and graded when developed. For example, if there was a small bump at one site of injection, the grade received was 1; if there was a more prominent bump, the grade received was 2; a small wound received a 3, a larger wound received a 4, continued bleeding received a 5, and anything abnormal or unknown received a 6 and was escalated to the veterinarian. For the final grade of each animal on a giving day, the scores were added together for each injection site (considering there are four sites), so a small bump on sites 1 and 2 resulted in a grade of 2 overall for that day, all animals were monitored daily (Monday – Friday).

Statistics

All results were expressed as mean ± SD with the level of statistical significance established at $p < 0.05$ for all statistics. All data was subjected to ROUT test to identify and exclude any outliers (Q=0.05). The D'Agostino-Pearson omnibus normality test was used to determine if data fit a normal Gaussian distribution. If data did fit a normal distribution, a non-parametric Kruskal-Wallis test was performed, this occurred when evaluating phase 2 % change of body weight, cage hangtime for all phases, raw EDL weights (phases 1 and 2), the cross-sectional area of MHC IIB, immune cell infiltration phase 1 of both the TA and DIA. A Kruskal-Wallis test was completed for respiration assessments of pyruvate malate for DIA state II, both -Cr and +Cr glutamate and succinate state III, and +Cr and -Cr for succinate state III for TA. When evaluating L-carnitine PCoA/Malate respiration, a Kruskal-Wallis test was also used for succinate state III evaluation. All other data not listed above had passed normality testing; thus, a parametric one-way ANOVA was completed. Multiple two-way ANOVAs were

completed; the first with factors of timepoint and treatment was used to determine specific interactions between ADP concentrations, and another two-way ANOVA was used to determine a main effect. This was completed in state III respiration in the pyruvate malate protocol of -Cr and +Cr DIA and -Cr TA, state III respiration in the L-Carnitine PCoA/Malate protocol of DIA, and H_2O_2 emissions of +Cr DIA. All other data not mentioned above failed normality testing and was then log-transformed, and the same two-way ANOVA testing were completed. If a significant interaction was observed, a Benjamini, Krieger, and Yekutieli post hoc test was completed to correct for the false discovery rate. All reported *p*-values are FDR-adjusted *p*-values (termed as '*q*'). All statistical analyses were performed with GraphPad Prism Software (Version 10. 0. 0. 131, La Jolla, CA, USA).

CHAPTER 5: RESULTS

Anthropometric Measures Elicits Insufficient Myositis Phenotype.

Compared to vehicle controls (GS), body weight was greater following myosin treatment (M) in phases 2 and 3 and greater following adjuvant treatment (GCI; ***Figure 6A-C***). Cage hang time was reduced following GCI treatment but unchanged in M for phases 1 and 2 (***Figure 6D-F***). There were no differences in grip strength between groups (***Figure 6G-I***) nor individual muscle weights (***Figure 6J-L***) in any phase.

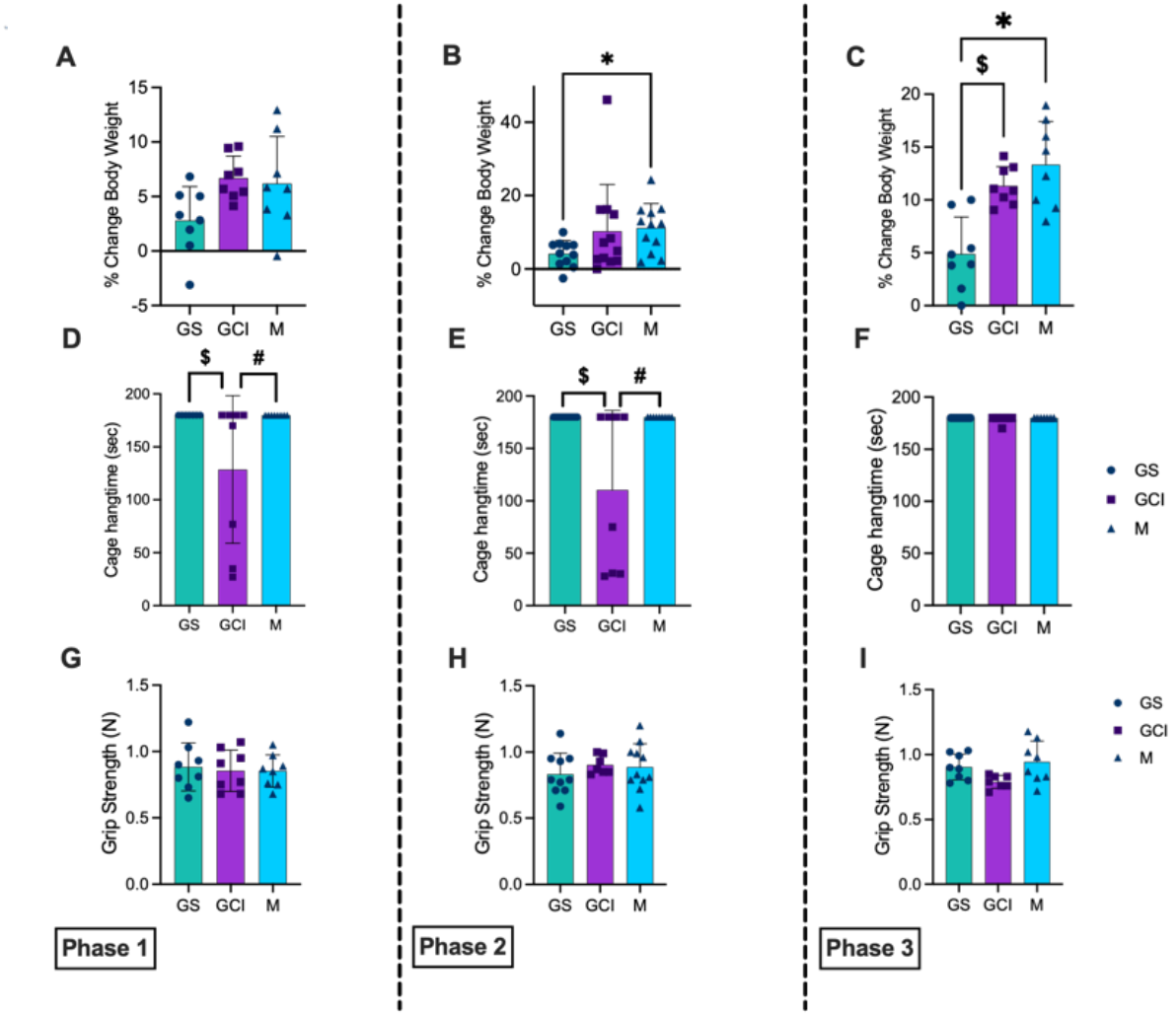

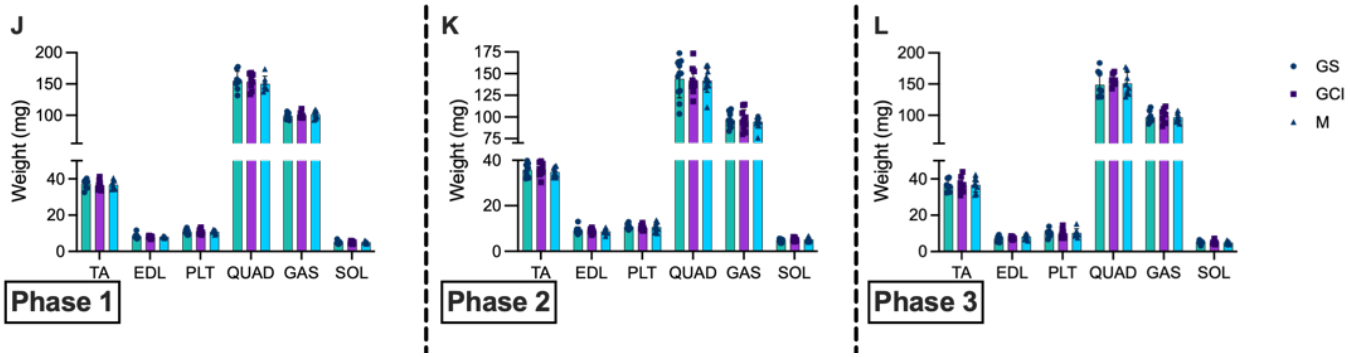

Figure 6. Anthropometric responses to adjuvant and myosin injections. Comparison of relative body weights across vehicle control (glycerol and saline; GS), adjuvant (glycerol, CFA, IFA) and myosin (M with vehicle and adjuvants) treatments in all phases (phase 1 (**A**), phase 2 (**B**), and phase 3 (**C**)), voluntary cage hangtime measured in all experimental groups in all phases (phase 1 (**D**), phase 2 (**E**), and phase 3 (**F**)), voluntary grip strength measured in all experimental groups in all phases (phase 1 (**G**), phase 2 (**H**), and phase 3 (**I**)), raw muscle weights across all experimental groups in all phases (phase 1 (**J**), phase 2 (**K**), and phase 3 (**L**)),. Measurements were performed after 3 injections (day 21; Phase 1) and 4 injections (day 28, Phase 2; day 49, Phase 3). Results represented as a mean ± SD; *n*=8-12; One-way ANOVA completed per graph (**A, C, G-I, J, K, L**), Kruskal-Wallis testing competed for (**B**, **D-F**, **J** EDL only, **K** EDL only); statistics demonstrating a main effect, $ P<0.05 compared GS to GCI, * P<0.05 compared GS to M, # P<0.05 GCI to M.

The presence of skin lesions was assessed to understand the impact of treatments on animal well-being. Compared to GS controls, lesion scores were the highest in the GCI and M group, where M exhibited greater lesions than GCI at multiple timepoints throughout each phase (***Figure 7A-C***), main effect not shown (P<0.05).

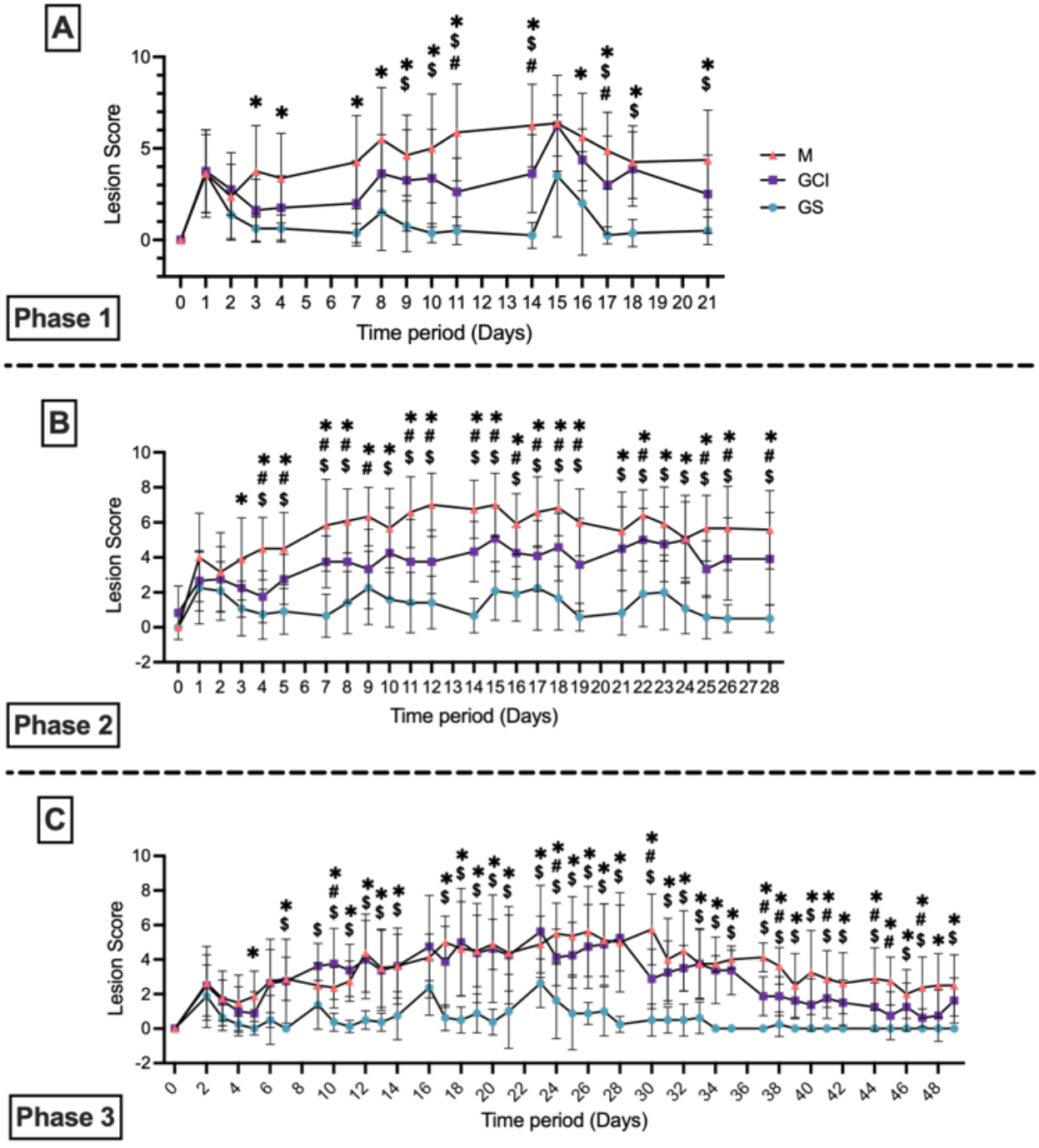

Figure 7. Myosin and adjuvant injections results in the development of skin lesions.

Animals are monitored daily (Monday – Friday), lesions were then compared after end point of vehicle control (glycerol and saline; GS), adjuvant (glycerol, CFA, IFA) and myosin (M with vehicle and adjuvants) treatments for all phases (phase 1 (**A**), phase 2 (**B**), and phase 3 (**C**)).

Results represented as a mean ± SD; *n*=8-12; Two-Way ANOVA completed to determine main effect, and specific effect at each timepoint; $ *P*<0.05 compared GS to GCI, * *P*<0.05 compared GS to M, # *P*<0.05 GCI to M.

Myosin treatment increases force production in the diaphragm and decreases force production in the tibialis anterior without changing cross-sectional area.

To determine force production, *in vitro* diaphragm force production and *in situ* TA force production was measured using a force frequency relationship in both phase 1 and phase 2. An increase in force production in GCI and M compared to GS was observed in phase 1 of the DIA, but restored to baseline in phase 2 (***Figure 8 A, B***). Interestingly in the TA a decrease in force production in M compared to both GCI and GS was determined in phase 1, this decrease also returned to baseline by phase 2 (***Figure 8 C, D***).

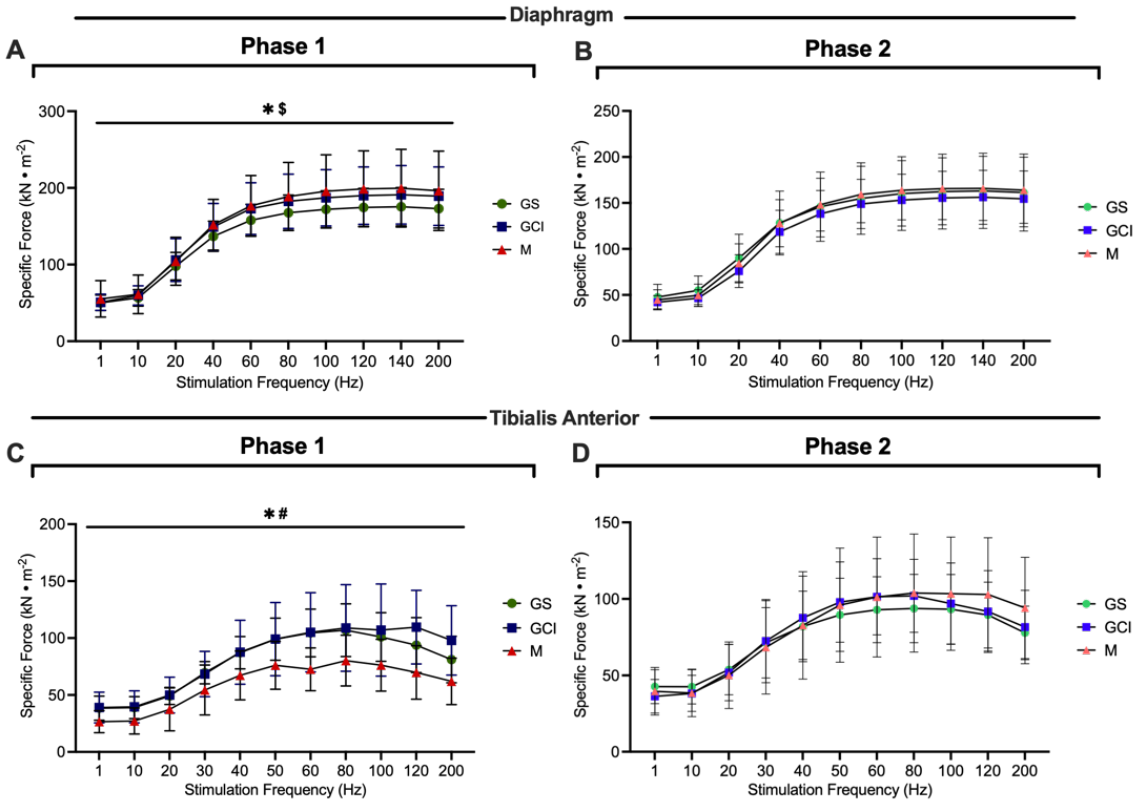

Figure 8. Force frequency increased in the diaphragm and decreased in the tibialis anterior, both recovering in phase 2. *In vitro* force frequency measures were evaluated in diaphragm in phase 1 (**A**) and recovered in phase 2 (**B**), and *in situ* force frequency measures decreased in tibialis anterior in both phase 1 (**C**) and recovered in phase 2 (**D**). Measurements were performed after 3 injections (day 21; Phase 1) and 4 injections (day 28, Phase 2) in vehicle control (glycerol and saline; GS), adjuvant (glycerol, CFA, IFA) and myosin (M with vehicle and adjuvants) treatments. Results represented as a mean ± SD; n=8-12; Two-way ANOVA to calculate main effect and frequency specific effects; statistics demonstrating main effect, $ P<0.05 compared GS to GCI, * P<0.05 compared GS to M, # P<0.05 GCI to M.

To assess if the above measures of weakness or strengthen of these muscles in phase 1 was due to muscle atrophy, cross-sectional area was assessed within each fiber type and compared across experimental groups. In the diaphragm there was no significant change in any fiber type in either phase 1 or phase 2 (***Figure 9 B, C***). In the tibialis anterior there was also no significant change in any fiber type in phase 1 (***Figure 9 E***). Tissue limitations prevented assessments of tibialis anterior in phase 2.

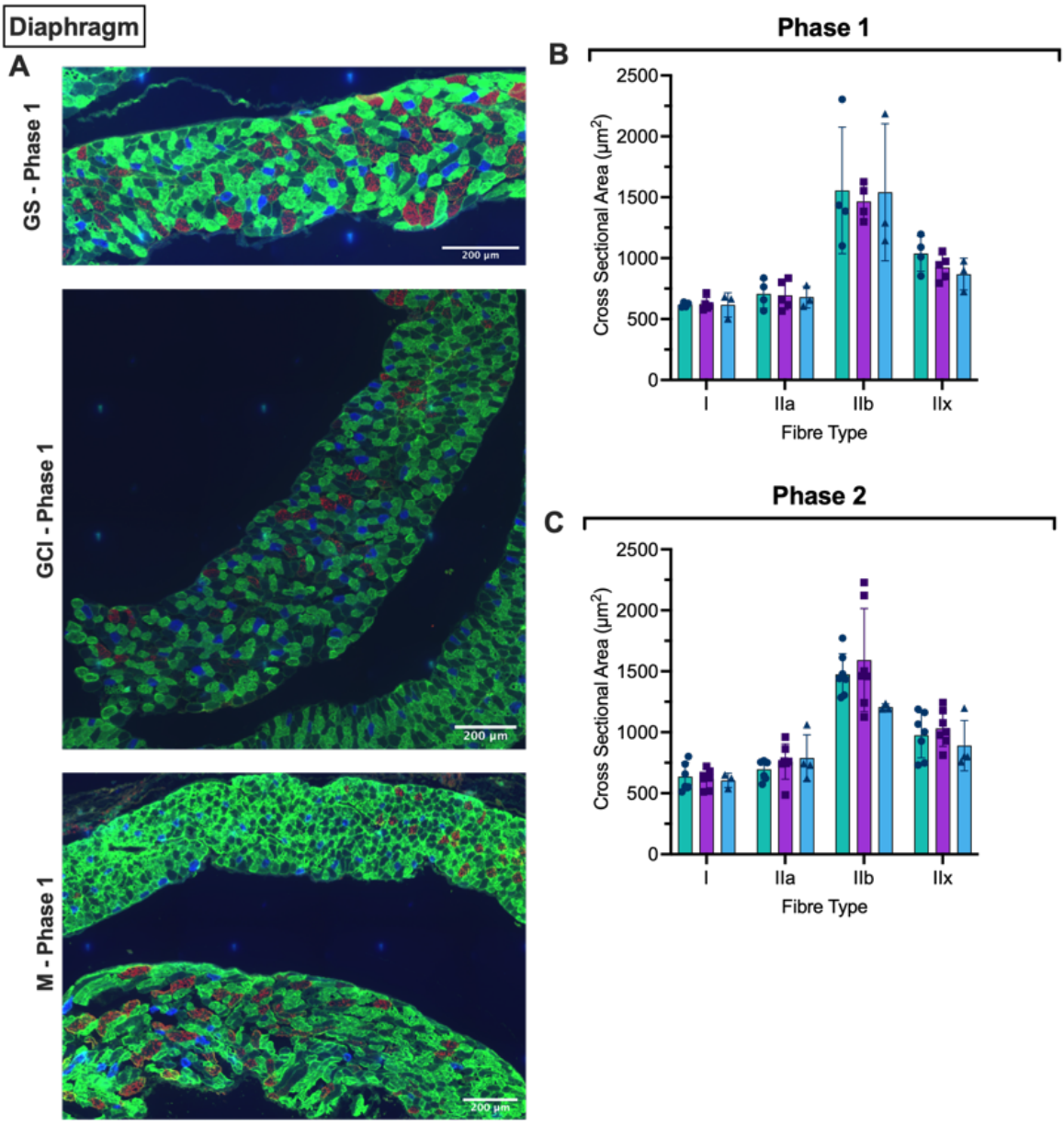
Diaphragm
A
GS - Phase 1
GCI - Phase 1
M - Phase 1
200 µm
200 µm
200 µm
B
Phase 1
Cross Sectional Area (µm²)
2500
2000
1500
1000
500
0
I
IIa
IIb
IIx
Fibre Type
C
Phase 2
Cross Sectional Area (µm²)
2500
2000
1500
1000
500
0
I
IIa
IIb
IIx
Fibre Type

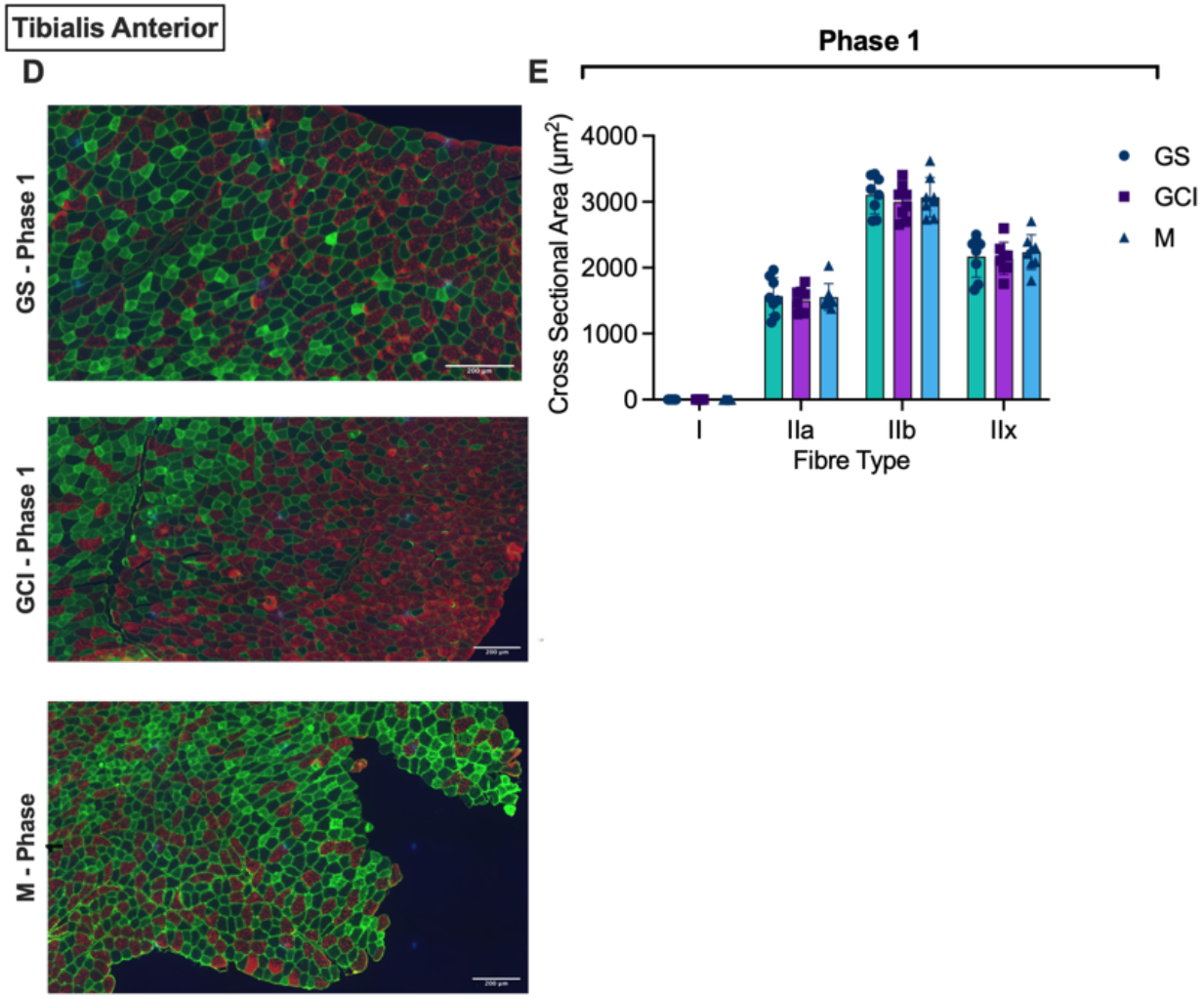

Figure 9. Muscle fiber type-specific cross-sectional area in diaphragm and tibialis anterior. Representative images of diaphragm muscle fibers stained for specific isoforms of myosin heavy chain (**A**). Histological images were quantified to calculate cross-sectional area of myosin heavy chain-specific fibers in phase 1 (**B**), and phase 2 (**C**). Representative images of the tibialis anterior muscle fibers stained the same as above (**D**). Images were then quantified to calculate cross-sectional area as above for phase 1 only (**E**) due to tissue limitations in phase 2. Measurements were performed after 3 injections (day 21; Phase 1) and 4 injections (day 28, Phase 2) in vehicle control (glycerol and saline; GS), adjuvant (glycerol, CFA, IFA) and myosin (M with vehicle and adjuvants) treatments. Results represented as a mean ± SD; *n*=8-12;

Individual one-way ANOVA completed for each fiber type for (**B, E, C**); Kruskal-Wallis test for fiber type IIB (**B**); statistics demonstrating a main effect, $ $P<0.05$ compared GS to GCI, * $P<0.05$ compared GS to M, # $P<0.05$ GCI to M.

Myosin treatment did not induce immune cell infiltration into skeletal muscle.

As muscle inflammation is a hallmark sign of myositis, immune cell infiltration was assessed by H&E staining. However, there were no differences in immune cell infiltration between all groups in either the diaphragm (***Figure 10***) or tibialis anterior (***Figure 11***). Tissue limitations prevented assessments of tibialis anterior in phases 2 and 3.

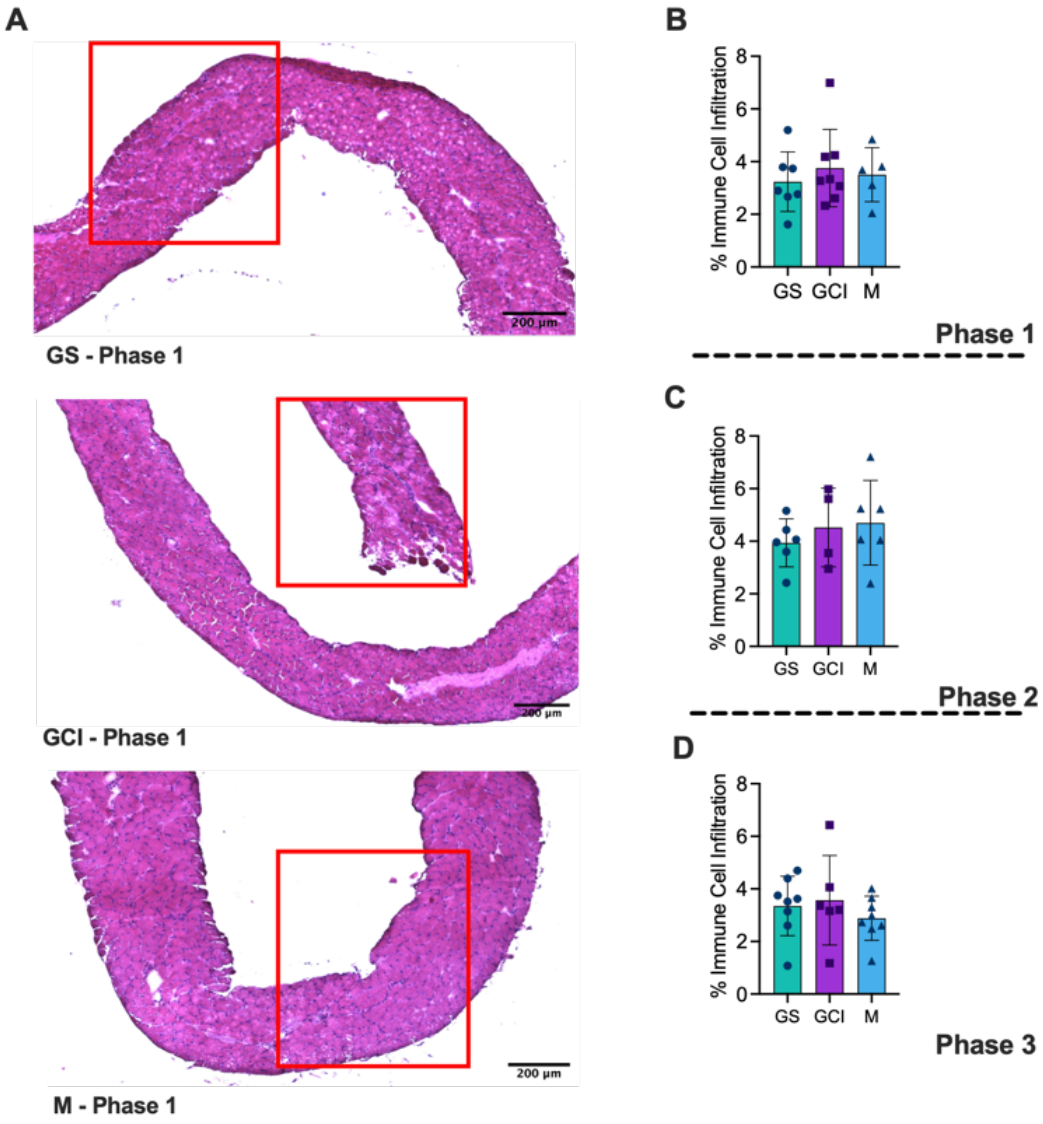

Figure 10. Myosin treatment had no impact on immune cell infiltration in the diaphragm. Representative images of diaphragm muscle highlighting immune cell infiltration used to quantify on Image J software **(A).** Skeletal muscle immune cell infiltration of the diaphragm muscle from phase 1 (**B**), phase 2 (**C**), and phase 3 (**D**) was assessed utilizing hematoxylin and eosin staining, comparison was made on all experimental groups. Measurements were performed after 3 injections (day 21; Phase 1) and 4 injections (day 28, Phase 2; day 49, Phase 3) in vehicle control (glycerol and saline; GS), adjuvant (glycerol, CFA, IFA) and myosin (M with vehicle and adjuvants) treatments. Results represented as a mean ± SD; *n*=8-12; One-way ANOVA

completed for (**C, D**), Kruskal-Wallis completed for (**B**); $ P<0.05 compared GS to GCI, * P<0.05 compared GS to M, # P<0.05 GCI to M.

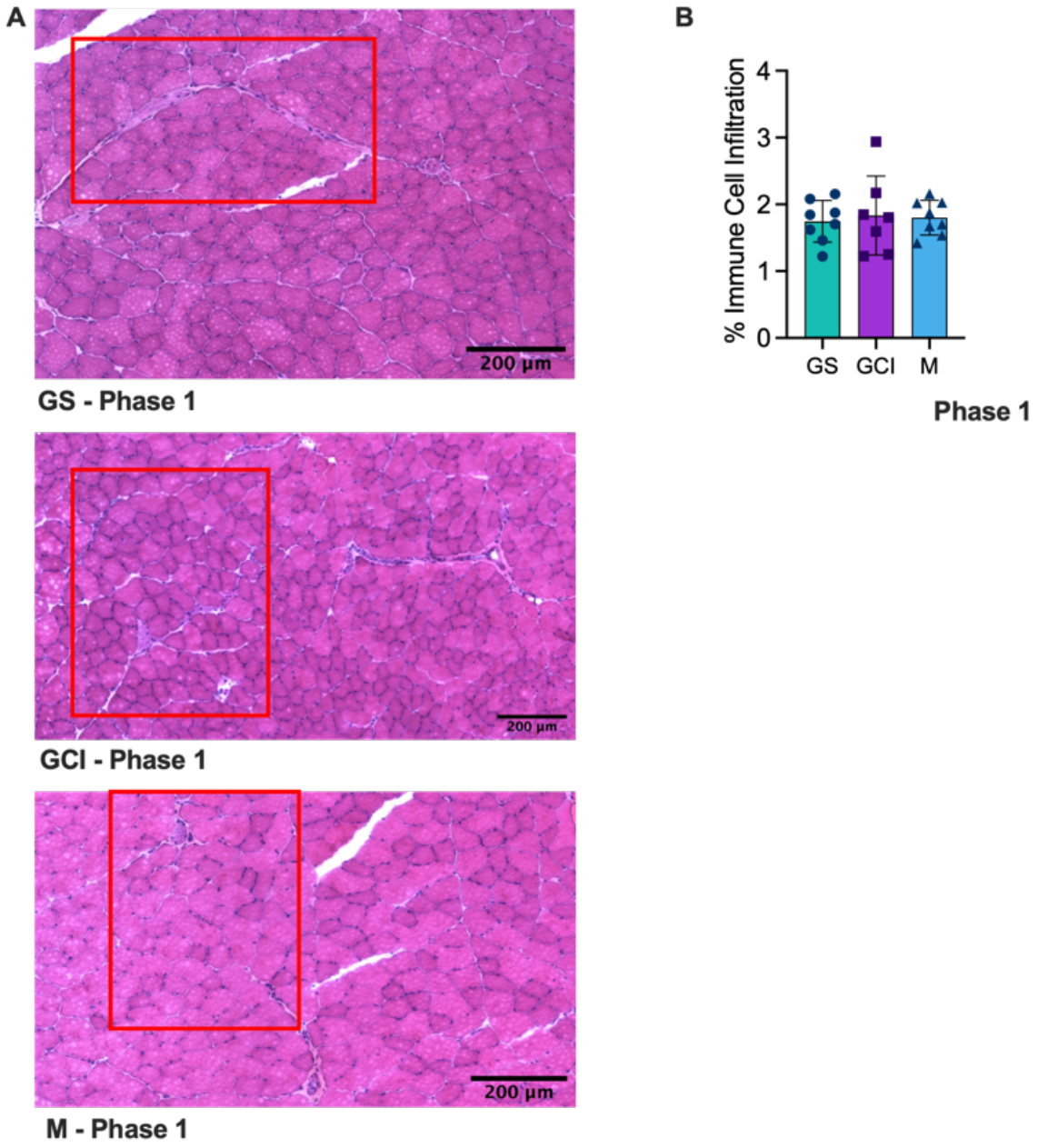

Figure 11. Myosin treatment had no impact on immune cell infiltration in the tibialis anterior. Representative images of tibialis anterior muscle highlighting immune cell infiltration used to quantify on Image J software **(A).** Skeletal muscle immune cell infiltration of the tibialis anterior muscle from phase 1 (**B**) was assessed utilizing hematoxylin and eosin staining,

comparison was made on all experimental groups. Measurements were performed after 3 injections (day 21; Phase 1) in vehicle control (glycerol and saline; GS), adjuvant (glycerol, CFA, IFA) and myosin (M with vehicle and adjuvants) treatments. Results represented as a mean ± SD; *n*=7-8; Kruskal-Wallis completed for **(B)**; $ *P*<0.05 compared GS to GCI, * *P*<0.05 compared GS to M, # *P*<0.05 GCI to M.

Mitochondrial respiration responses vary in a tissue- and substrate-specific manner

As previous literature has identified a mitochondrial dysfunction within the EAM model[3], we wanted to evaluate if our PT-free model could mimic these findings. In the DIA we determined that state III respiration was lower in the GCI and M group compared to GS only in the absence of creatine (-Cr) (***Figure 12F***). There was no difference identified between any groups when evaluated state II respiration (***Figure 12 A, E***) or glutamate and succinate-supported state III respiration (***Figure 12 C, D, G, H***).

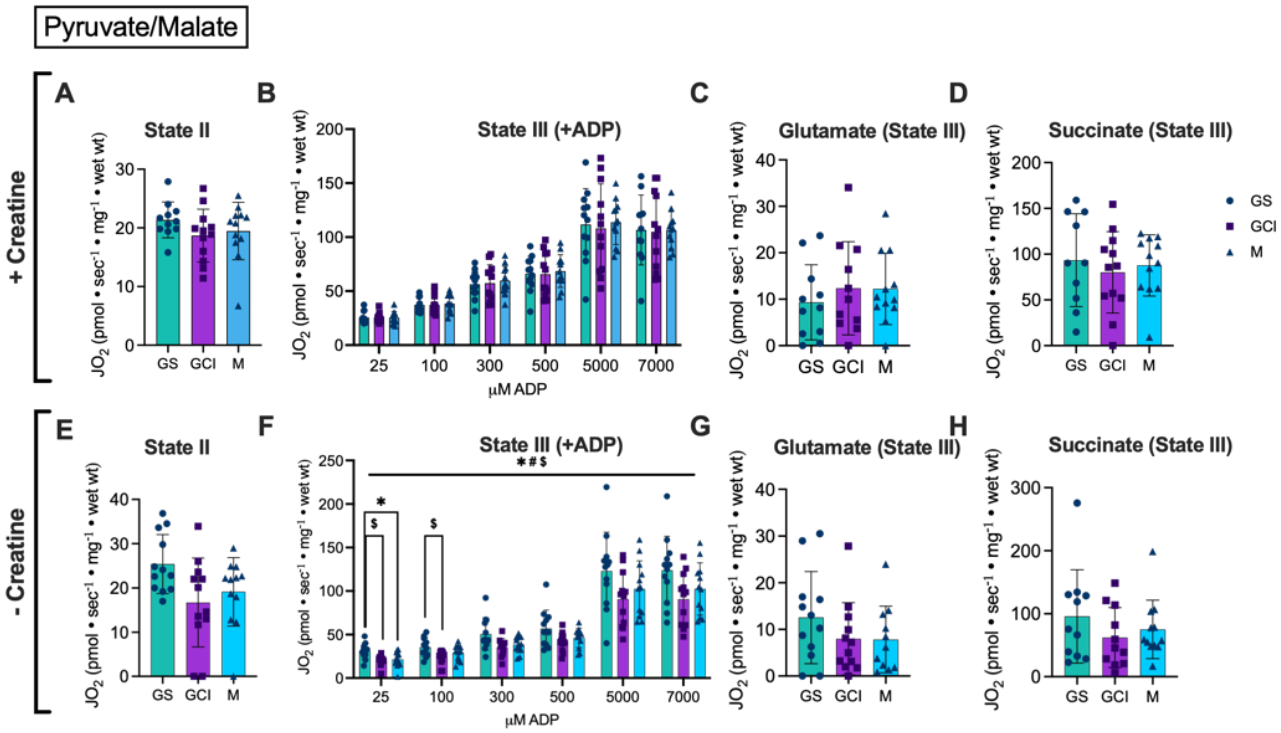

Figure 12. Myosin treatment lowered respiration in creatine independent (-Cr) state III mitochondrial respiration in the diaphragm. Complex I stimulated respiration in the diaphragm with +Cr (**A-D**), and without - Cr (**E-H**). Measurements were performed after 4 injections (day 28, Phase 2) in vehicle control (glycerol and saline; GS), adjuvant (glycerol, CFA, IFA) and myosin (M with vehicle and adjuvants) treatments. Results represented as a mean ± SD; n=12; Kruskal-Wallis test completed for (**A, E, G, H**), One-way ANOVA completed for (**C, D**), two-way ANOVA to calculate main effect and titration specific effects (**B, F**); main effect shown on graph, $ P<0.05 compared GS to GCI, * P<0.05 compared GS to M, # P<0.05 GCI to M.

The above experiment was duplicated in the TA, which demonstrated a decrease in state III respiration in the M group compared to GS control in the presences of creatine (+Cr), but lower than GCI in the absences of creatine (-Cr) (***Figure 13 B, F***). There was no difference identified between any groups when evaluated state II respiration (***Figure 13 A, E***) or glutamate and succinate-supported state III respiration (***Figure 13 C, D, G, H***).

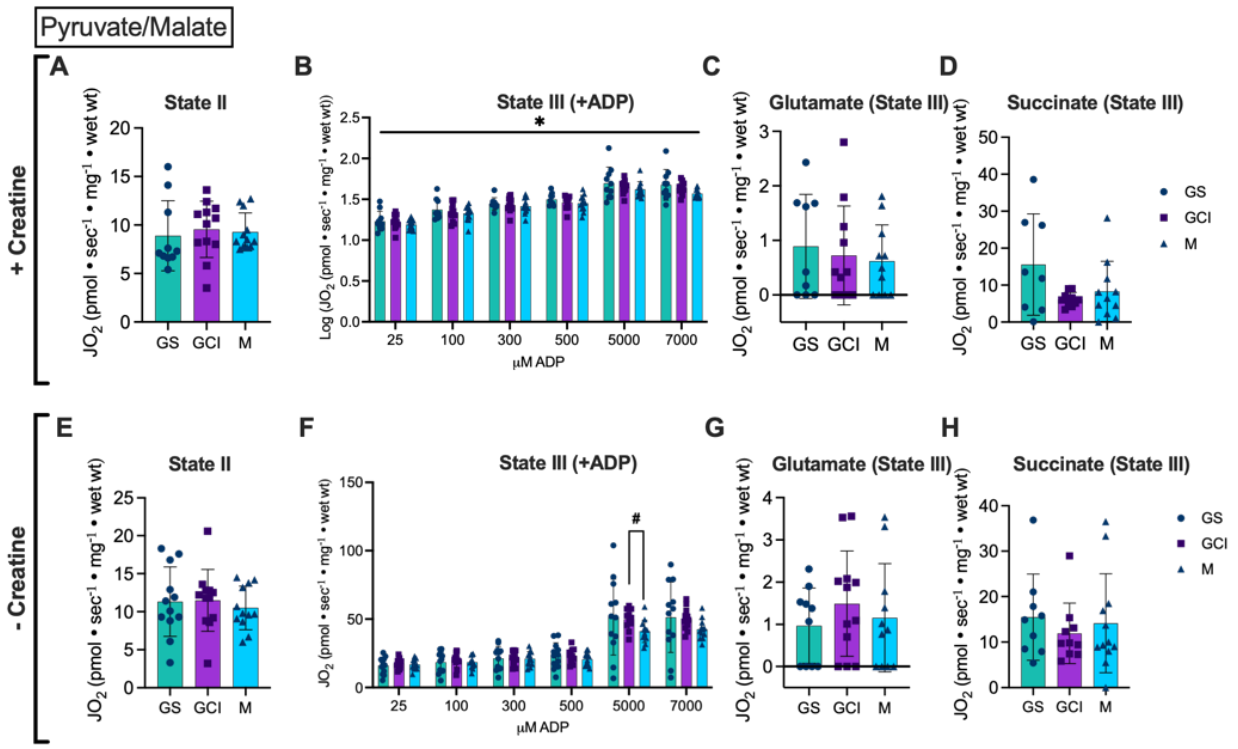

Figure 13. Myosin treatment lowered respiration in creatine independent (-Cr) and creatine dependent (+Cr) state III mitochondrial respiration in the tibialis anterior. Complex I stimulated respiration in the diaphragm with +Cr (**A-D**), and without - Cr (**E-H**). Measurements were performed after 4 injections (day 28, Phase 2) in vehicle control (glycerol and saline; GS), adjuvant (glycerol, CFA, IFA) and myosin (M with vehicle and adjuvants) treatments. Results represented as a mean ± SD; *n*=12; One-way ANOVA completed for (**A, C, E, G**), Kruskal-Wallis completed for (**D, H**), Log transformed (**B**) and regular (**F**) two-way ANOVA to calculate main effect and titration specific effects; $ P<0.05 compared GS to GCI, * P<0.05 compared GS to M, # P<0.05 GCI to M, main effect denoted in (**B**), titration specific effect denoted in (**F**) no main effect present.

We then evaluated fatty acid stimulated mitochondrial respiration in the DIA and TA in a creatine dependent (+Cr) pathway. Which demonstrated no difference between any groups when

evaluated state II respiration (***Figure 14 A, D***) or ADP, glutamate, and succinate-supported state III respiration (***Figure 14 B, C, E, F***).

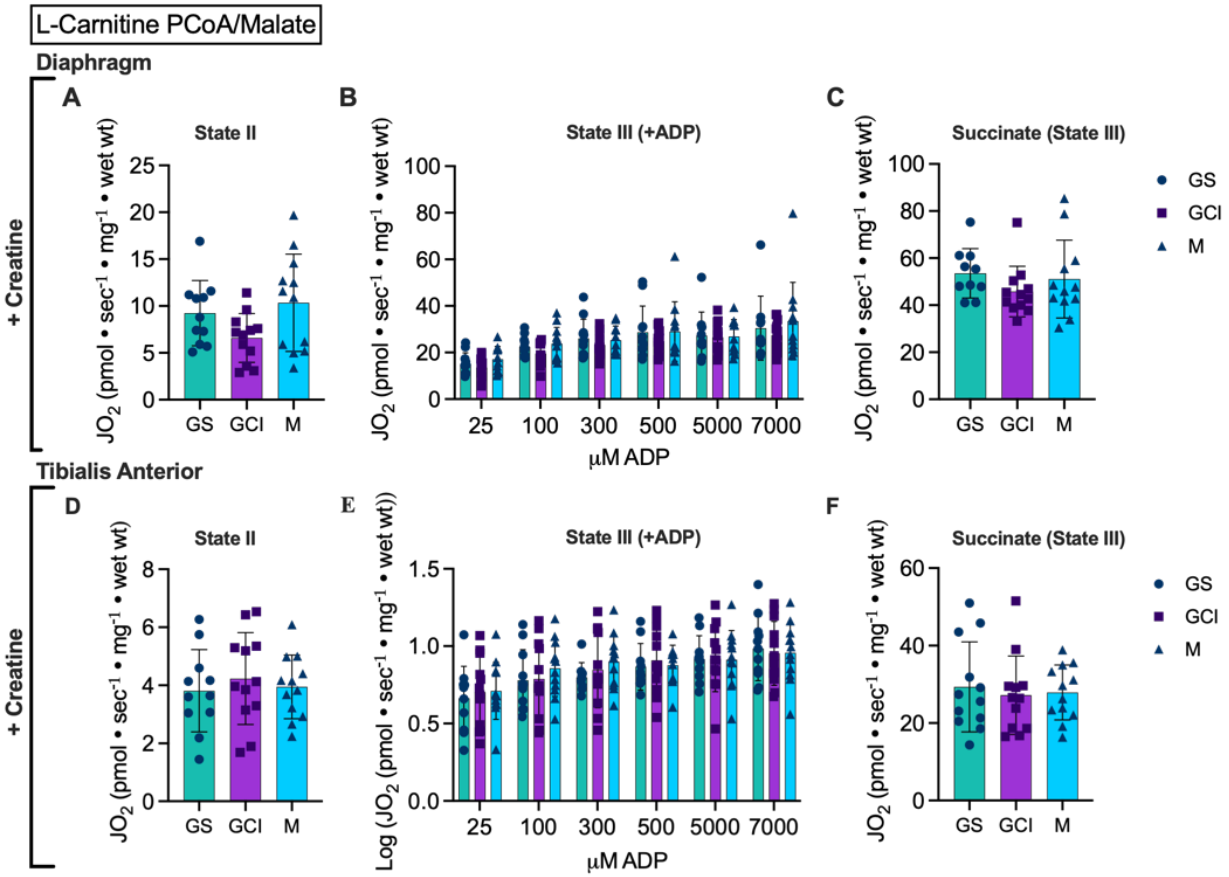

Figure 14. Myosin treatment did not impact respiration in creatine dependent (+Cr) fatty acid stimulated mitochondrial respiration. Fatty acid oxidation substrates used to stimulate respiration in the diaphragm (**A-C**) and the tibialis anterior (**D-F**). Measurements were performed after 4 injections (day 28, Phase 2) in vehicle control (glycerol and saline; GS), adjuvant (glycerol, CFA, IFA) and myosin (M with vehicle and adjuvants) treatments. Results represented as a mean ± SD; n=12; One-way ANOVA completed for (**A, D, F**), Kruskal-Wallis completed for (**C**), Log transformed (**E**) and regular (**B**) two-way ANOVA to calculate main effect and titration specific effects; $ P<0.05 compared GS to GCI, * P<0.05 compared GS to M, # P<0.05 GCI to M.

Impact on mitochondrial H_2O_2 emissions (mH_2O_2) varies in tissue and substrate specific manner.

We then evaluated mitochondrial H_2O_2 emissions under a variety of conditions, to verify if the previously identified increase in mH_2O_2 was occurring in complex I or complex II supported mitochondrial H_2O_2 emissions, as well as if mtCK influenced this process in any way. Complex II supported (10 mM succinate) mH_2O_2 emissions in the presences and absences of ADP and creatine was completed in both the diaphragm and tibialis anterior. In the diaphragm, there was no significant change seen in the +Cr or -Cr (***Figure 15 A-D***).

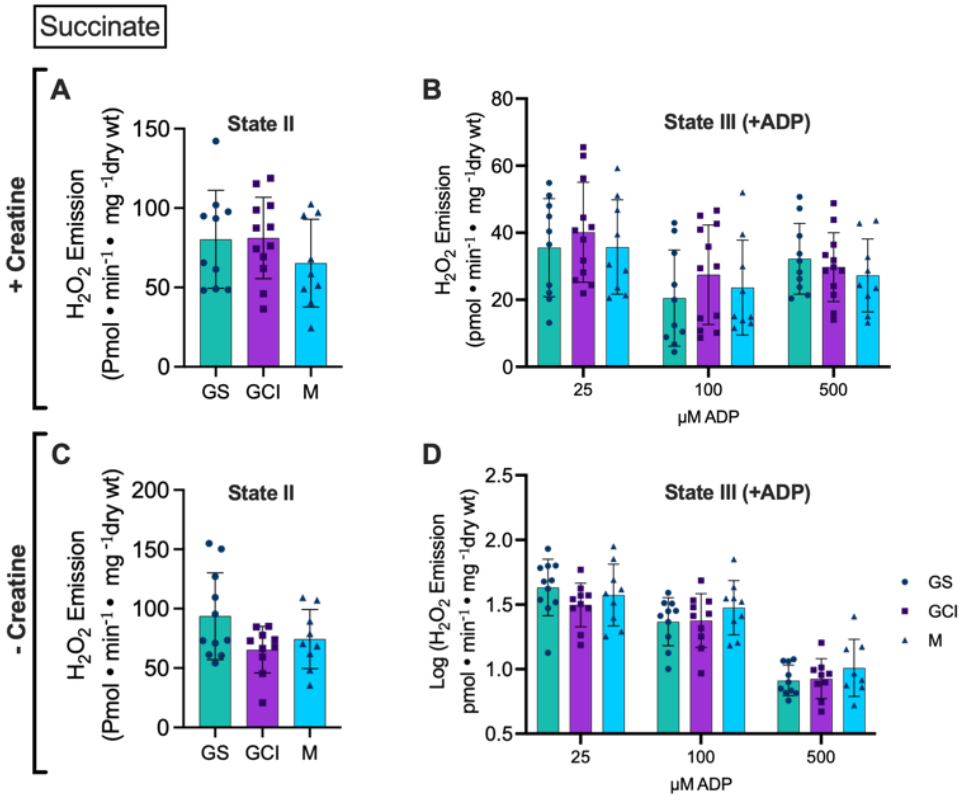

Figure 15. Myosin treatment did not impact diaphragm mH_2O_2 in creatine dependent (+Cr) or independent (-Cr) Mitochondrial H_2O_2 emissions. Complex II stimulated H_2O_2 emissions in the diaphragm with +Cr (**A, B**), and without - Cr (**C, D**). Measurements were performed after 4 injections (day 28, Phase 2) in vehicle control (glycerol and saline; GS),

adjuvant (glycerol, CFA, IFA) and myosin (M with vehicle and adjuvants) treatments. Results represented as a mean ± SD; *n*=12; One-way ANOVA completed for (**A, C**), Log transformed (**D**) and regular (**B**) two-way ANOVA to calculate main effect and titration specific effects; $ *P*<0.05 compared GS to GCI, * *P*<0.05 compared GS to M, # *P*<0.05 GCI to M.

We then evaluated mitochondrial H_2O_2 emissions under the same conditions in the tibialis anterior. There was no difference identified between any groups when evaluated state II mH_2O_2 (***Figure 16 A, C***). In presences of Cr an interesting increase in M and GS mH_2O_2 compared to the adjuvant group GCI was identified (***Figure 16 B***). In the -Cr pathway a surprising decrease of mH_2O_2 was established in M group when compared to GS control only (***Figure 16D***).

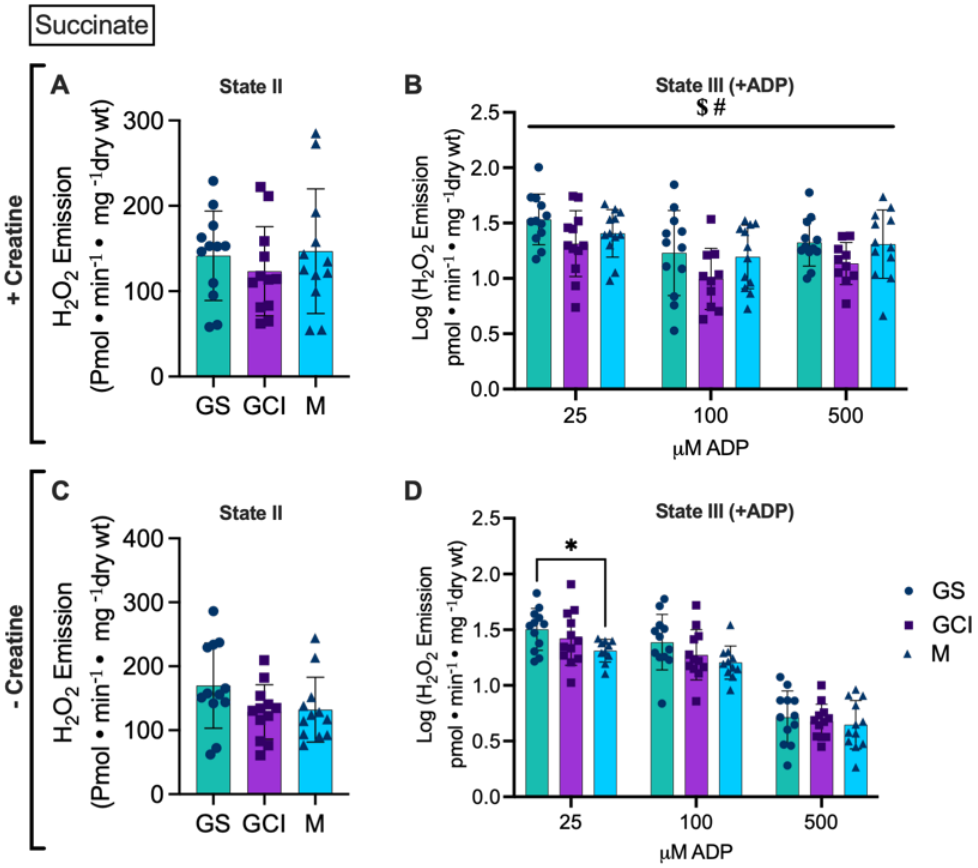

Figure 16. Myosin treatments impacted tibialis anterior mH_2O_2 in differing ways in creatine dependent (+Cr) or independent (-Cr) Mitochondrial H_2O_2 emissions. Complex II stimulated H_2O_2 emissions in the tibialis anterior with +Cr (**A, B**), and without - Cr (**C, D**). Measurements were performed after 4 injections (day 28, Phase 2) in vehicle control (glycerol and saline; GS), adjuvant (glycerol, CFA, IFA) and myosin (M with vehicle and adjuvants) treatments. Results represented as a mean ± SD; n=12; One-way ANOVA completed for (**A, C**), regular two-way ANOVA to calculate main effect and titration specific effects (**B, D**); $ P<0.05 compared GS to GCI, * P<0.05 compared GS to M, # P<0.05 GCI to M.

Evaluating complex I supported mH_2O_2 was evaluated to allowing us to determine if mH_2O_2 emissions is substrate specific in this myosin treatment model. We utilized complex I supported (10 mM pyruvate and 2 mM malate) mH_2O_2 emissions in presences of creatine in both the diaphragm and tibialis anterior. There was no difference identified between any groups when evaluated state II mH_2O_2 (***Figure 17 A, C***). In the presences of ADP an increase in mH_2O_2 in the GCI control group compared to the GS control group, in the diaphragm was established (***Figure 17 B***). In tibialis anterior an increase in mH_2O_2 in the M group compared to both controls (***Figure 17 D***).

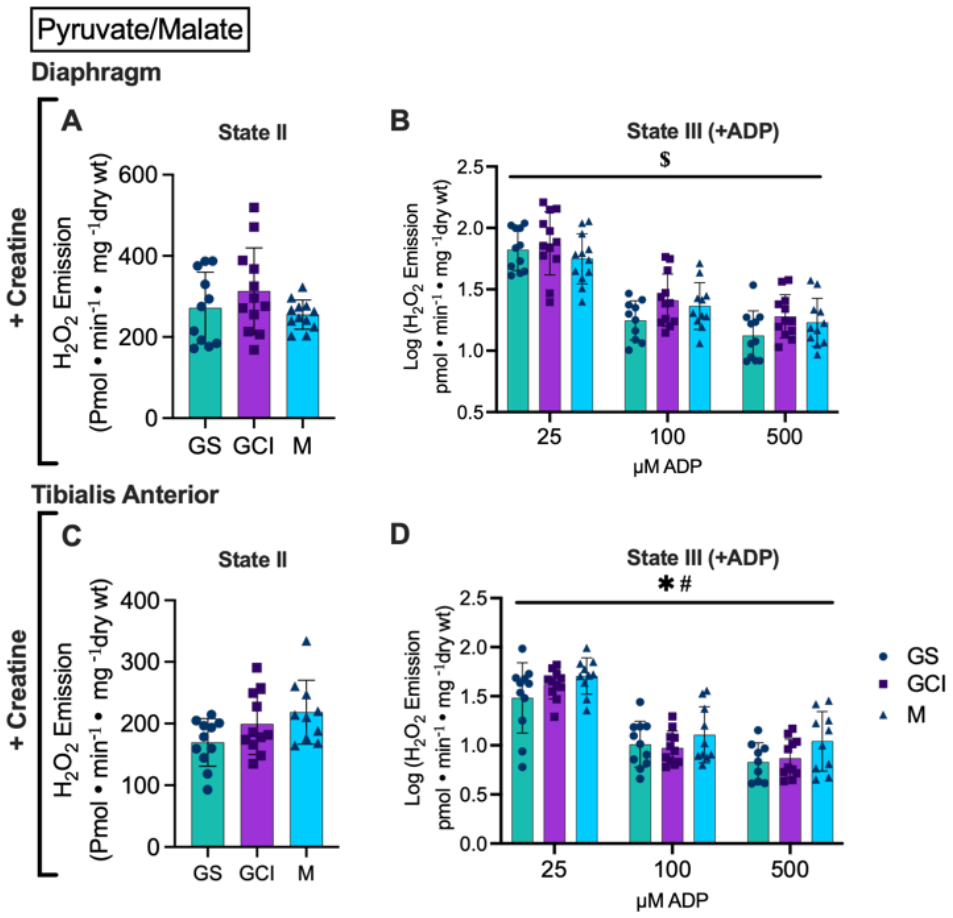

Figure 17. Myosin treatments impacted mH$_2$O$_2$ in creatine dependent (+Cr) Mitochondrial H$_2$O$_2$ emissions. Complex I stimulated H_2O_2 emissions in the diaphragm (**A, B**) and the tibialis anterior (**C, D**), evaluated in phase 2 only. Measurements were performed after 4 injections (day 28, Phase 2) in vehicle control (glycerol and saline; GS), adjuvant (glycerol, CFA, IFA) and myosin (M with vehicle and adjuvants) treatments. Results represented as a mean ± SD; *n*=12; One-way ANOVA completed for (**C**), Kruskal-Wallis completed for (**A**), Log transformed two-way ANOVA to calculate main effect and titration specific effects (**B, D**); $ *P*<0.05 compared GS to GCI, * *P*<0.05 compared GS to M, # *P*<0.05 GCI to M.

CHAPTER 6: DISCUSSION

6.1 *Muscle Alterations Induced by Myosin Injections*

A main objective of this study was to determine if repeated myosin and adjuvant injections in the absences of pertussis toxin (PT-free) decreases force production in the diaphragm and tibialis anterior in a time-dependent manner, and if weakness occurs with or independent of atrophy. Identified in Figure 8 A and B, an increase in the diaphragm force production was seen in phase 1 for both the myosin treated and adjuvant treated groups but returned to baseline in phase 2. This indicates adjuvant injections induced a diaphragm-specific adaptation for increased force production. But when cross-sectional area was evaluated, there was no impact to fiber size in either phase 1 or phase 2. Interestingly Figure 8 C and D, a decrease was identified in force production of only the myosin treated group in the tibialis anterior in phase 1 that was then recovered to baseline in phase 2. This weakness identified in phase 1 was independent of atrophy as cross-sectional area of the tibialis anterior was not impacted by these injections. Thus, indicating myosin injections induced a tibialis anterior-specific adaptation for decrease force production, which is contradictory to the evidence outlined from the diaphragm. Thus, an increase in number of injections within this model does not amplify disease progression in the diaphragm or in the tibialis anterior.

Interestingly, within the human condition of myositis there is a respiratory involvement that is frequently associated with IIMs. Interstitial Lung Disease (ILD) is an overarching term for disease induced fibrosis of the lungs[64]. Manifestations of ILD are often associated with the presences of anti-SRP autoantibody in patients, which are part of the anti-synthetase autoantibody family, although ILD has never previously been reported in the animal model of EAM[65,64]. In humans idiopathic pulmonary fibrosis (most frequent diagnosed ILD) the key

restriction to lung function has been identified as the reduction of the lungs ability to expand, where chest wall compliance and respiratory muscle strength is often preserved[66, 67]. Due to the fibrosis development making lung expansion difficult these respiratory muscles may be preserved due to the increased force required to produce normal lung expansion resulting in a selective "training stimulus" or hormetic response[68]. Thus, the increase in muscle strength see in the diaphragm for this model in the absences of changes to fiber cross-sectional area may be due to a hormetic response preserving muscle strength. If present in this model the fibrosis of the lungs could be demanding more of the muscle resulting in that muscle adaptation. A suggested improvement in the manifestation of this condition over time can be an explanation for the recovery seen by phase 2.

Considering muscle weakness is an expected symptom of myositis, and in some cases is associated with muscle atrophy another interesting cause of this muscle weakness could be contractile dysfunction. Contractile dysfunction is a common cause of weakness in individuals impacted by chronic inflammatory diseases[69], it is the loss of specific force and may cause weakness in the absence of atrophy[69]. Potential pathways causing contractile dysfunction in chronic inflammatory conditions have suggested that pro-inflammatory cytokines are released into systemic circulation where they impact skeletal muscle function[69]. These pro-inflammatory cytokines include IL-6, C-reactive protein, and tumor necrosis factor (TNF)[69]. Some studies have also identified that reactive oxygen and nitrogen species may also play a role in contractile dysfunction[69]. As outlined previously, TNF-α and IL-6 have important roles in assisting in muscle cell proliferation but in excess impact skeletal muscle proliferation and function significantly. TNF-α and IL-6 along with other pro-inflammatory cytokines have been proven to be upregulated in patients with myositis (DM/PM)[70]. Although our study was unable to evaluate

these cytokines mentioned, this provides insight on potential mechanisms that cause the results we observed and can lead to further investigations. Thus, the decrease in force production in the tibialis anterior independent of atrophy measured in phase 1 can potentially be attributed to contractile dysfunction that recovered in phase 2 similarly to what was seen in the diaphragm.

Although this PT-free EAM model does not induce the characteristic anthropometric measures (Figure 6 A-L) expected of this model, there is a clear muscle manifestation at phase 1 that impacts the diaphragm and tibialis anterior separately and when considering manifestations of the human condition can be attributed to characteristic myositis manifestations. Thus, to further explore the myositis manifestations of our model investigation of the extent of mitochondrial impact was evaluated.

6.2 *Exploring Mitochondrial Function in PT-free EAM*

An additional main objective of this thesis was to determine if repeated myosin and adjuvant injections alter mitochondrial respiration or H_2O_2 emissions in a muscle-specific manner in this PT-free EAM model. Outlined in Figure 12 F, in a creatine independent pathway (-Cr) a decrease in complex I stimulated respiration in the diaphragm was demonstrated in the adjuvant and myosin group compared to the control. When evaluating mitochondrial H_2O_2 emissions (mH_2O_2) within the diaphragm using complex I – supported substrates an increase in the adjuvant group was demonstrated in the presences of creatine compared to the control (Figure 17 B). Conversely, in the tibialis anterior a decrease in complex I stimulated respiration was demonstrated in myosin treated group compared to the adjuvant control (creatine independent pathway, Figure 13 F), and myosin treated group was lower than the glycerol saline control (creatine dependent pathway, Figure 13 B). Whereas in the tibialis anterior complex II-supported substrates demonstrated lower mH_2O_2 in myosin group compared to the glycerol saline

control (creatine independent pathway, Figure 16 D) and higher mH_2O_2 in the myosin group compared to the adjuvant control (creatine dependent pathway, Figure 16 B). Our findings thus confirmed that our PT-free EAM model altered mitochondrial respiration and H_2O_2 emissions in a muscle-specific manner.

In conditions with chronic inflammation like IIMs resulting in circulating cytokines, these cytokines often impact other functions of the body. As mentioned above cytokines like TNF-α and IL-6 are upregulated in patients with myositis[70]. It has been identified in cells treated with TNF-α, that exposure causes dose-dependent mitochondrial dysfunction displayed as a decrease in mitochondrial respiration[55]. It has also been identified that pro-inflammatory cytokines can activate mitochondrial-induced apoptosis leading to cell death[71]. Similarly, IL-6 overexpression triggers increase Drp-1 protein expression, resulting in an increase of mitochondrial fragmentation which impacts mitochondrial function by increasing mitophagy[2023-09-05 5:00:00 PM,57]. An increase of mitophagy due to an over expression of TNF-α and IL-6, and an increase in mitochondrial fragmentation due to IL-6 overexpression would greatly impact mitochondrial function and likely increase superoxide production. Thus, the decrease in mitochondrial respiration and increase in mitochondrial H_2O_2 emissions in the diaphragm and tibialis anterior may be attributed to the increase in circulating cytokines impacting mitochondrial function within this model, although we were unable to identify cytokine presences. There was no creatine effect demonstrated, therefore cytosolic and mitochondrial creatine kinase is clearly not impacted by these circulating cytokines, but mitochondrial function is. These circulated cytokines impacted mitochondrial function, thus determining the extent of immune cell infiltration demonstrated in our PT-free EAM model was the next objective.

6.3 *Perspective in Immune Cell Infiltration Findings*

A major drive for the design of this study was to identify if an EAM model was inducible in wildtype animals with the absences of pertussis toxin (PT). In order to indicate a successful model of EAM, muscle specific infiltrations were evaluated as well as other crude measures of successful EAM induction (muscle weights, grip strength, cage hangtime). Anthropometric measures demonstrated an adjuvant effect on cage hangtime in phases 1 and 2 (Figure 6 D, E) and an increase in the percent change in body weight in the myosin group in phases 2 and 3 (Figure 6 B, C). Considering other EAM literature has identified decreases in body weight or muscle weight in PT induced EAM, these results directly contradict these findings[20]. Immune cell infiltration into the diaphragm was assessed across all time points (Figure 10A-D) and demonstrated no change in infiltrates across any groups. Similarly, the tibialis anterior was assessed for infiltrates at phase 1 and demonstrated no change across any of the groups (Figure 11 A, B).

This PT-free model of EAM was partially influenced by animal ethics restrictions, due to the additive effects of the adjuvant and PT impacting animal welfare. Outline in previous sections PT is known to induce systemic inflammation in other animal models that worsens the disease phenotype[23]. Other EAM literature that did not utilize PT did so in a mouse strain that is prone to spontaneous myopathy from a splice-site mutation in the dysferlin gene[25]. When autoantibody production was evaluated in PT induced EAM, the autoantibodies that are known to be upregulated in the human condition were not present in the animal model[7]. This indicated that even PT induced EAM may not be a sufficient model to mimic disease mechanisms of human myositis. These results support that a PT-free EAM model is not effectively inducible in a wildtype animal without the presence of PT, as the systemic inflammation produced by PT

injections amplifies the myositis phenotype. Although a myositis phenotype is still outlined in some of the results presented it is not as aggressive as other literature and thus is an insufficient model when compared to the human condition.

CHAPTER 7: CONCLUSION AND FUTURE DIRECTIONS

7.1 *Conclusion*

There is little known about the mechanism of disease onset in human myositis patients, but myositis specific autoantibodies impact symptom presentation in some cases. To explore the human condition, investigational animal models like the experimental autoimmune myositis model are utilized. Currently, this mouse model of autoimmune myositis is often induced using injections of foreign myosin protein combined with an adjuvant and pertussis toxin (PT) to promote an immunological response. However, PT can induce systemic inflammation which casts doubts on whether such models induce myositis through autoimmunity to the myosin antigen or simply in response to systemic inflammation. Additionally, questions are raised if this model exemplifies the mechanism of induction enough to be comparable to the human condition. Thus, this thesis used a PT-free induction technique of exposing mice to rabbit-derived myosin and identified an increase in diaphragm force production with an interesting muscle-specific adjuvant effect. Additionally, this study also identified a decrease in TA force production that recovers over time without atrophy, and decreases in mitochondrial respiration as well as increases in mitochondrial H_2O_2 emissions in both tissues. These findings demonstrate that the myosin antigen alone induces a mild myositis phenotype. This finding also implies that in order to fully induce this EAM model, PT is required to activate systemic inflammation and exacerbate the phenotype. The requirement of PT within this model demonstrates a limitation when attempting to compare to the human condition, as the autoimmune condition triggers chronic inflammation by the production of autoantigens and antibodies that are not present in this animal model. Thus, this study underscores the need to further develop more robust models of this disease.

7.2 *Future Directions and Limitations*

A major limitation of this study is the lack of a pertussis toxin experimental group, this is due to ethical limitations. A PT experimental group would allow us to determine the full impact on muscle and mitochondrial function and allow us to make confirmed conclusion between the PT-free and PT-induced EAM models. Also, allowing us to confirm that the EAM model is only inducible in wildtype animals in the presence of PT. Another limitation to this model was the use of IFA as the adjuvant substitute in injections 2, 3, and 4. Considering CFA (Freund's Complete Adjuvant) is an affective and aggressive adjuvant, the use of CFA was only permitted by research ethics for 1 injection per animal. When evaluating EAM literature, models are often induced by multiple injections thus the substitution of IFA (Freund's Incomplete adjuvant) was made. This is a limitation because although still an adjuvant, IFA lacks the mycobacterium to assist in facilitating that strong immune response. Although other EAM models have used IFA within their injections[7], they do so with the presence of PT which would still stimulate a strong immune response.

A better model for exploring the mechanisms of myositis needs to be utilized for therapy development. The PT-free EAM model is not a sufficient model and thus is not comparable to the human condition. A major future direction for the field would be to develop a model that utilized myositis specific autoantigens and autoantibodies to really encapsulate what is known of the human disease. There is also a need to establish circulating and tissue-infiltrating cytokines in models that do and do not use pertussis toxin which will assist in interpretations of the EAM model.

CHAPTER 8: REFERENCES

1. Malik, A., Hayat, G., Kalia, J. S. & Guzman, M. A. Idiopathic Inflammatory Myopathies: Clinical Approach and Management. *Front. Neurol.* **7**, (2016).
2. Barsotti, S. & Lundberg, I. E. Current Treatment for Myositis. *Curr Treat Options in Rheum* **4**, 299–315 (2018).
3. Meyer, A. *et al.* IFN-β-induced reactive oxygen species and mitochondrial damage contribute to muscle impairment and inflammation maintenance in dermatomyositis. *Acta Neuropathol* **134**, 655–666 (2017).
4. Clark, A. *et al. CCAC guidelines on antibody production*. (Canadian Council on Animal Care, 2002).
5. Bittner, R. E. *et al.* Dysferlin deletion in SJL mice (SJL-Dysf) defines a natural model for limb girdle muscular dystrophy 2B. *Nat Genet* **23**, 141–142 (1999).
6. Suzuki, F. *et al.* Inhibition of CX3CL1 (Fractalkine) Improves Experimental Autoimmune Myositis in SJL/J Mice1. *The Journal of Immunology* **175**, 6987–6996 (2005).
7. Allenbach, Y. *et al.* Role of Regulatory T Cells in a New Mouse Model of Experimental Autoimmune Myositis. *The American Journal of Pathology* **174**, 989–998 (2009).
8. Milone, M. Diagnosis and Management of Immune-Mediated Myopathies. *Mayo Clinic Proceedings* **92**, 826–837 (2017).
9. Callen, J. P. & Wortmann, R. L. Dermatomyositis. *Clinics in Dermatology* **24**, 363–373 (2006).
10. Amato, A. A. & Greenberg, S. A. Inflammatory Myopathies: *CONTINUUM: Lifelong Learning in Neurology* **19**, 1615–1633 (2013).
11. Fiorentino, D., Marvi, U. & Chung, L. Clinical presentation and evaluation of dermatomyositis. *Indian J Dermatol* **57**, 375 (2012).
12. Milisenda, J. C., Selva-O'Callaghan, A. & Grau, J. M. The diagnosis and classification of polymyositis. *Journal of Autoimmunity* **48–49**, 118–121 (2014).
13. Pinal-Fernandez, I., Casal-Dominguez, M. & Mammen, A. L. Immune-Mediated Necrotizing Myopathy. *Curr Rheumatol Rep* **20**, 21 (2018).
14. Greenberg, S. A. Inclusion body myositis: clinical features and pathogenesis. *Nat Rev Rheumatol* **15**, 257–272 (2019).
15. Oddis, C. V. & Aggarwal, R. Treatment in myositis. *Nat Rev Rheumatol* **14**, 279–289 (2018).
16. Hodgkinson, L. M., Wu, T. T. & Fiorentino, D. F. Dermatomyositis autoantibodies: how can we maximize utility? *Ann Transl Med* **9**, 433–433 (2021).
17. Ghirardello, A. *et al.* Autoantibodies in Polymyositis and Dermatomyositis. *Curr Rheumatol Rep* **15**, 335 (2013).
18. Allenbach, Y., Benveniste, O., Stenzel, W. & Boyer, O. Immune-mediated necrotizing myopathy: clinical features and pathogenesis. *Nat Rev Rheumatol* **16**, 689–701 (2020).
19. Suber, T. L., Casciola-Rosen, L. & Rosen, A. Mechanisms of Disease: autoantigens as clues to the pathogenesis of myositis. *Nat Rev Rheumatol* **4**, 201–209 (2008).

20. Yamada, T. *et al.* Improved skeletal muscle fatigue resistance in experimental autoimmune myositis mice following high-intensity interval training. *Arthritis Res Ther* **24**, 156 (2022).
21. Connelly, C. E., Sun, Y. & Carbonetti, N. H. Pertussis Toxin Exacerbates and Prolongs Airway Inflammatory Responses during Bordetella pertussis Infection. *Infect Immun* **80**, 4317–4332 (2012).
22. Shive, C. L., Hofstetter, H., Arredondo, L., Shaw, C. & Forsthuber, T. G. The enhanced antigen-specific production of cytokines induced by pertussis toxin is due to clonal expansion of T cells and not to altered effector functions of long-term memory cells. *Eur. J. Immunol.* **30**, 2422–2431 (2000).
23. Zou, M. *et al.* Pertussis toxin–induced inflammatory response exacerbates intracerebral haemorrhage and ischaemic stroke in mice. *Stroke Vasc Neurol* **7**, 29–37 (2022).
24. Ohyanagi, N. *et al.* Retinoid ameliorates experimental autoimmune myositis, with modulation of Th cell differentiation and antibody production in vivo. *Arthritis Rheum* **60**, 3118–3127 (2009).
25. Eckardt, R., Carstens, E. & Fiedler, W. [Synthesis of new beta 1-receptor blockaders]. *Pharmazie* **30**, 633–637 (1975).
26. Bhatti, G. K. *et al.* Targeting mitochondrial bioenergetics as a promising therapeutic strategy in metabolic and neurodegenerative diseases. *Biomedical Journal* **45**, 733–748 (2022).
27. Moyes, C. D. & Le Moine, C. M. R. TISSUE RESPIRATION | Mitochondrial Respiration. in *Encyclopedia of Fish Physiology* 959–965 (Elsevier, 2011). doi:10.1016/B978-0-12-374553-8.00121-0.
28. Sharma, L., Lu, J. & Bai, Y. Mitochondrial Respiratory Complex I: Structure, Function and Implication in Human Diseases. *CMC* **16**, 1266–1277 (2009).
29. Tiidus, P. M., Tupling, A. R., Houston, M. E. & Houston, M. E. *Biochemistry primer for exercise science*. (Human Kinetics, 2012).
30. Dröse, S. & Brandt, U. Molecular Mechanisms of Superoxide Production by the Mitochondrial Respiratory Chain. in *Mitochondrial Oxidative Phosphorylation* (ed. Kadenbach, B.) vol. 748 145–169 (Springer New York, 2012).
31. Kowaltowski, A. J., de Souza-Pinto, N. C., Castilho, R. F. & Vercesi, A. E. Mitochondria and reactive oxygen species. *Free Radical Biology and Medicine* **47**, 333–343 (2009).
32. Sies, H. & Jones, D. P. Reactive oxygen species (ROS) as pleiotropic physiological signalling agents. *Nat Rev Mol Cell Biol* **21**, 363–383 (2020).
33. Nordberg, J. & Arnér, E. S. J. Reactive oxygen species, antioxidants, and the mammalian thioredoxin system1 1This review is based on the licentiate thesis “Thioredoxin reductase—interactions with the redox active compounds 1-chloro-2,4-dinitrobenzene and lipoic acid” by Jonas Nordberg, 2001, Karolinska Institute, Stockholm, ISBN 91-631-1064-4. *Free Radical Biology and Medicine* **31**, 1287–1312 (2001).
34. Schlattner, U., Tokarska-Schlattner, M. & Wallimann, T. Mitochondrial creatine kinase in human health and disease. *Biochimica et Biophysica Acta (BBA) - Molecular Basis of Disease* **1762**, 164–180 (2006).

35. Gash, M. C., Kandle, P. F., Murray, I. V. & Varacallo, M. Physiology, Muscle Contraction. in *StatPearls* (StatPearls Publishing, 2023).
36. Willingham, T. B., Ajayi, P. T. & Glancy, B. Subcellular Specialization of Mitochondrial Form and Function in Skeletal Muscle Cells. *Front. Cell Dev. Biol.* **9**, 757305 (2021).
37. Hoppeler, H. *et al.* Endurance training in humans: aerobic capacity and structure of skeletal muscle. *Journal of Applied Physiology* **59**, 320–327 (1985).
38. Gandra, P. G., Nogueira, L. & Hogan, M. C. Mitochondrial activation at the onset of contractions in isolated myofibres during successive contractile periods: NAD(P)H and mitochondrial membrane potential during contractions. *The Journal of Physiology* **590**, 3597–3609 (2012).
39. Hargreaves, M. & Spriet, L. L. Skeletal muscle energy metabolism during exercise. *Nat Metab* **2**, 817–828 (2020).
40. Bellissimo, C. & Perry, C. Regulation of Skeletal Muscle Reactive Oxygen Species During Exercise. in *The Routledge Handbook on Biochemistry of Exercise* (2020).
41. Mailloux, R. J. An Update on Mitochondrial Reactive Oxygen Species Production. *Antioxidants* **9**, 472 (2020).
42. Barbieri, E. & Sestili, P. Reactive Oxygen Species in Skeletal Muscle Signaling. *Journal of Signal Transduction* **2012**, 1–17 (2012).
43. Costamagna, D., Costelli, P., Sampaolesi, M. & Penna, F. Role of Inflammation in Muscle Homeostasis and Myogenesis. *Mediators of Inflammation* **2015**, 1–14 (2015).
44. Londhe, P. & Guttridge, D. C. Inflammation induced loss of skeletal muscle. *Bone* **80**, 131–142 (2015).
45. Acharyya, S. *et al.* TNF Inhibits Notch-1 in Skeletal Muscle Cells by Ezh2 and DNA Methylation Mediated Repression: Implications in Duchenne Muscular Dystrophy. *PLoS ONE* **5**, e12479 (2010).
46. Villalta, S. A., Deng, B., Rinaldi, C., Wehling-Henricks, M. & Tidball, J. G. IFN-γ Promotes Muscle Damage in the mdx Mouse Model of Duchenne Muscular Dystrophy by Suppressing M2 Macrophage Activation and Inhibiting Muscle Cell Proliferation. *The Journal of Immunology* **187**, 5419–5428 (2011).
47. Scheller, J., Chalaris, A., Schmidt-Arras, D. & Rose-John, S. The pro- and anti-inflammatory properties of the cytokine interleukin-6. *Biochimica et Biophysica Acta (BBA) - Molecular Cell Research* **1813**, 878–888 (2011).
48. Ahmed, T. A. *et al.* Interleukin-6 inhibits growth hormone-mediated gene expression in hepatocytes. *American Journal of Physiology-Gastrointestinal and Liver Physiology* **292**, G1793–G1803 (2007).
49. Qualls, A. E., Southern, W. M. & Call, J. A. Mitochondria-cytokine crosstalk following skeletal muscle injury and disuse: a mini-review. *American Journal of Physiology-Cell Physiology* **320**, C681–C688 (2021).
50. Grazioli, S. & Pugin, J. Mitochondrial Damage-Associated Molecular Patterns: From Inflammatory Signaling to Human Diseases. *Front. Immunol.* **9**, 832 (2018).

51. Zhou, R., Yazdi, A. S., Menu, P. & Tschopp, J. A role for mitochondria in NLRP3 inflammasome activation. *Nature* **469**, 221–225 (2011).
52. Warren, G. L. *et al.* Mechanisms of skeletal muscle injury and repair revealed by gene expression studies in mouse models. *The Journal of Physiology* **582**, 825–841 (2007).
53. Liprandi, A., Bartoli, C., Figarella-Branger, D., Pellissier, J.-F. & Lepidi, H. Local expression of monocyte chemoattractant protein-1 (MCP-1) in idiopathic inflammatory myopathies. *Acta Neuropathologica* **97**, 642–648 (1999).
54. Tierney, M. T. *et al.* STAT3 signaling controls satellite cell expansion and skeletal muscle repair. *Nat Med* **20**, 1182–1186 (2014).
55. Doll, D. N., Rellick, S. L., Barr, T. L., Ren, X. & Simpkins, J. W. Rapid mitochondrial dysfunction mediates TNF-alpha-induced neurotoxicity. *Journal of Neurochemistry* **132**, 443–451 (2015).
56. Fix, D. K., VanderVeen, B. N., Counts, B. R. & Carson, J. A. Regulation of Skeletal Muscle DRP-1 and FIS-1 Protein Expression by IL-6 Signaling. *Oxidative Medicine and Cellular Longevity* **2019**, 1–12 (2019).
57. Kobayashi, S. *et al.* Mitochondrial Fission and Mitophagy Coordinately Restrict High Glucose Toxicity in Cardiomyocytes. *Frontiers in Physiology* **11**, (2020).
58. Van Der Burgh, R. *et al.* Defects in Mitochondrial Clearance Predispose Human Monocytes to Interleukin-1β Hypersecretion. *Journal of Biological Chemistry* **289**, 5000–5012 (2014).
59. Okiyama, N. *et al.* Experimental myositis inducible with transfer of dendritic cells presenting a skeletal muscle C protein-derived CD8 epitope peptide. *International Immunology* **27**, 327–332 (2015).
60. Jacques, A. M. *et al.* The molecular phenotype of human cardiac myosin associated with hypertrophic obstructive cardiomyopathy. *Cardiovascular Research* **79**, 481–491 (2008).
61. Hughes, M. C. *et al.* Early myopathy in Duchenne muscular dystrophy is associated with elevated mitochondrial H_2O_2 emission during impaired oxidative phosphorylation. *Journal of Cachexia, Sarcopenia and Muscle* **10**, 643–661 (2019).
62. Delfinis, L. J. *et al.* Muscle weakness precedes atrophy during cancer cachexia and is linked to muscle-specific mitochondrial stress. *JCI Insight* **7**, e155147 (2022).
63. Perry, C. G. R. *et al.* Inhibiting myosin-ATPase reveals a dynamic range of mitochondrial respiratory control in skeletal muscle. *Biochemical Journal* **437**, 215–222 (2011).
64. Ge, Y. *et al.* Interstitial lung disease is not rare in immune-mediated necrotizing myopathy with anti-signal recognition particle antibodies. *BMC Pulm Med* **22**, 14 (2022).
65. Kuwana, M., Gil-Vila, A. & Selva-O'Callaghan, A. Role of autoantibodies in the diagnosis and prognosis of interstitial lung disease in autoimmune rheumatic disorders. *Therapeutic Advances in Musculoskeletal* **13**, 1759720X2110324 (2021).
66. Laurent Plantier *et al.* Physiology of the lung in idiopathic pulmonary fibrosis. *EUROPEAN RESPIRATORY REVIEW* **27**, 170062 (2018).

67. DiMarco, A. F., Kelsen, S. G., Cherniack, N. S. & Gothe, B. Occlusion Pressure and Breathing Pattern in Patients with Interstitial Lung Disease [1, 2]. *Am Rev Respir Dis* **127**, 425–430 (1983).
68. Lands, L. C., Heigenhauser, G. J. F. & Jones, N. L. Respiratory and Peripheral Muscle Function in Cystic Fibrosis. *Am Rev Respir Dis* **147**, 865–869 (1993).
69. Powers, S. K., Lynch, G. S., Murphy, K. T., Reid, M. B. & Zijdewind, I. Disease-Induced Skeletal Muscle Atrophy and Fatigue. *Medicine & Science in Sports & Exercise* **48**, 2307–2319 (2016).
70. Lopez De Padilla, C. *et al.* Interferon-regulated chemokine score associated with improvement in disease activity in refractory myositis patients treated with rituximab. *Clinical and Experimental Rheumatology* **33**, 655–663 (2015).
71. Huang, Y., Erdmann, N., Peng, H., Zhao, Y. & Zheng, J. The role of TNF related apoptosis-inducing ligand in neurodegenerative diseases. *Cell Mol Immunol* **2**, 113–122 (2005).
72. Heeger, P. S. *et al.* Revisiting Tolerance Induced by Autoantigen in Incomplete Freund's Adjuvant. *The Journal of Immunology* **164**, 5771–5781 (2000).

SUPPLEMENTAL FIGURES

Coomassie Gel

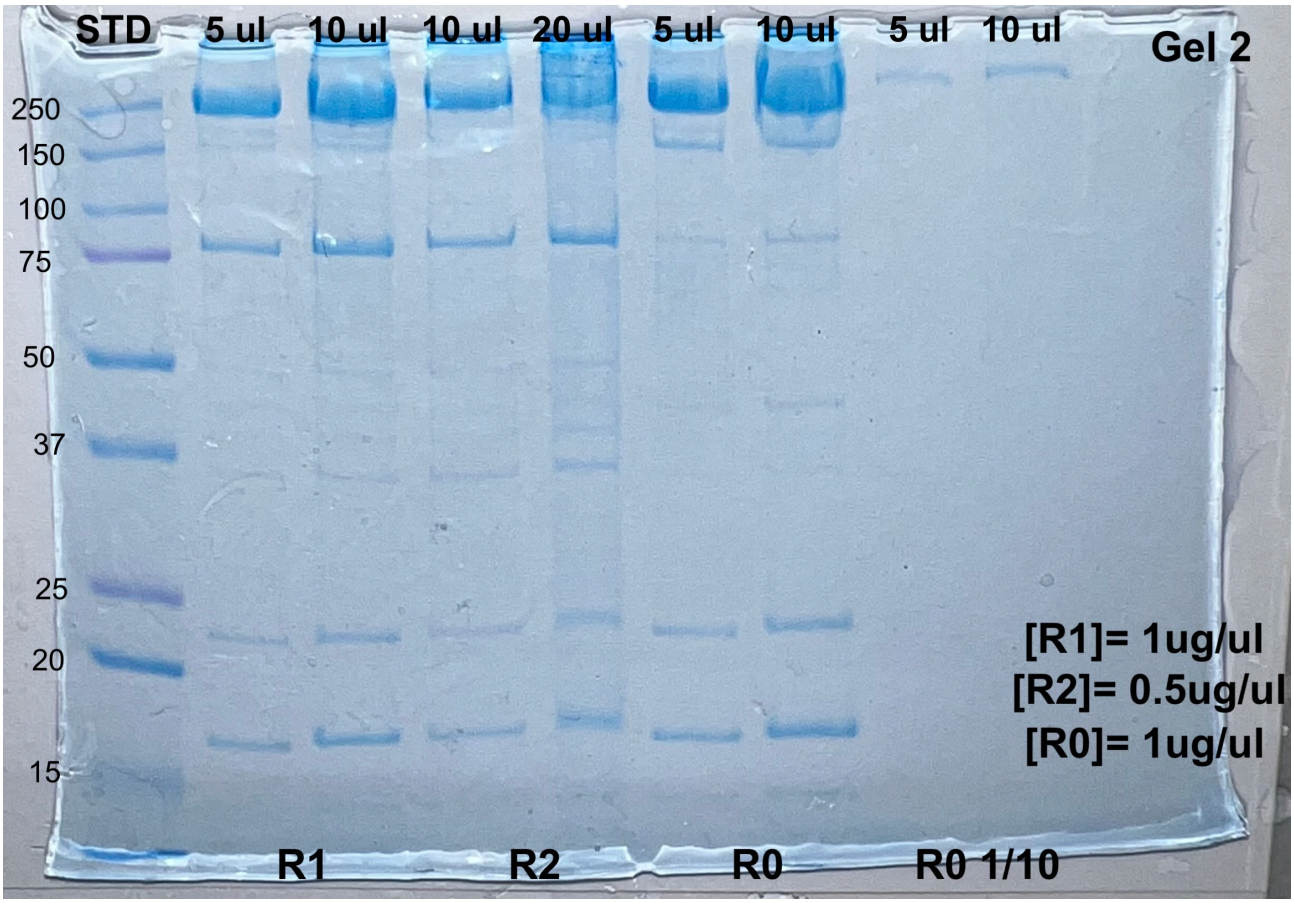

Supplemental Figure 1. Coomassie gel demonstrating purification of myosin used for injections. (Injections used a mix of R0+R1+R2). On gel stain which does not require transfer picture of gel taken with iPhone. Image not quantified used for comparison of previous purifications. R0= Rabbit 0 (myosin purification 1); R1= Rabbit 1 (myosin purification 2); R2= Rabbit 2 (myosin purification 3); R0 1/10= Rabbit 0 (diluted to 1:10); STD= Protein Standard

APPENDIX A: Myosin Purification Protocol

SKELETAL/CARDIAC MUSCLE MYOSIN PREP

Protocol Provided by Dr. Leslie Anna Leinwand of University of Colorado Boulder, 2022

Note: The maximum yield is 1% of muscle weight

All procedures should be carried out in the cold room on ice

All equipment and solutions need to be precooled.

This prep is for 1 rabbit. Adding a second rabbit is feasible, though doing so adds a significant amount of solution volume (may be problematic during centrifugation steps) and time to the prep as a whole. Plan accordingly.

Day 1 (6-8 hours):

Prepared: Buffers A and B, 50 mls of 0.2 M EDTA. Coordinate centrifuge times for days 2 and 3.

Materials:

Large tray

Meat grinder

Blades

Scissors

Saran wrap

Large beaker with stir bar

Cold water jug

Bucket of ice

Place all items in the cold room so that they are available at the start of the dissection. Add DTT and ATP to buffers A and B, as specified. Also place 2 liters of acetone in the cold room if planning on preparing acetone powder.

SKELETAL: Remove pectoralis muscle from a freshly killed rabbit, trying to remove the top layer of muscle as a whole. Wrap in Saran wrap and keep on ice. Remove the tendons and outer fascia from the muscle and chop the tissue into half- to quarter-inch pieces.

CARDIAC: Remove the left ventricle from freshly killed pig heart. Chop into half inch pieces. Pass through a pre-chilled meat grinder that has been rinsed with **0.2 M EDTA**, collecting the ground tissue in a weigh boat. Re-grind and remove tissue from inside grinder.

Weigh tissue Wt. = _____ g

Add 2 ml of **buffer A** per gram of tissue.

1st volume added = _____ ml buffer A

Total volume: _____ ml

(e.g. tissue weight = 100g, 1st and total volume = 200 ml)

Stir gently with a large stir bar for **12 minutes**. The stirring time matters; do not let this mixture sit indefinitely.

Add an equal amount of cold ddH_2O quickly to stop the reaction.

2nd volume added = _____ ml cold ddH_2O

Total volume: _____ ml

(e.g. 1st vol. = 200 ml, 2nd vol. will equal 200 ml, total = 400 ml)

Add cold ddH_2O to dilute to half again (solution is now ¼ x).

3rd volume added = _____ ml cold ddH_2O

Total volume: _____ ml

(e.g. total was 400 ml, 3rd volume is 400 additional ml, total is now 800 ml = 4x 1st volume)

Filter through 4 layers of cheesecloth into a 4L beaker (a large graduated cylinder works well, too). Be prepared to change the cheesecloth if necessary.

Slowly add cold ddH_2O to precipitate the protein, diluting to a final concentration of 1/10.

1st volume added X 6 = _____ ml cold ddH_2O

Total volume: _____ ml

(e.g. 1st volume = 200 ml, x 6 = 1200 ml, + current 800 ml = 2000 ml = 10x original volume)

Add protease inhibitor cocktail. For BioVision Protease Inhibitor Cocktail (cat # K 271-500), dilute stock to 1x, add 1.5 **ul** per 500 **mls** of solution.

Cover and let the precipitate settle in the cold room. This step may take 3 to 4 hours, with the precipitate settling slowly at first, and then abruptly forming a layer at the bottom of the beaker. Check every 30 minutes or so. During this downtime, prepare **buffer C** and keep it in the cold room or refrigerator. This is also a good time to move on to the acetone powder prep using the pulp from the filter step (see "Preparation of Acetone Powder from Rabbit Skeletal Muscle").

After the precipitate has settled, siphon off as much clear liquid as possible. Be careful not to take any of the precipitate.

Centrifuge the precipitate in a SLA-3000 rotor (holds 6, 500 ml tubes) at 8,000 rpm (RCF = 10816 g) for 10 minutes at 4^{o} C.

Discard the supernatant and soak the pellet in a minimal amount of **buffer B** while preparing for dialysis, then gently resuspend (solution should be thick).

Dialyze overnight against 4 L of **buffer C** at 4^{o} C.

Day 2 (5-6 hours):

Materials:

Large beaker with stir bar

Cold ddH20 water jug

Bucket of ice

Centrifuge tubes (~ 25 ml. Check compatibility with the rotor you intend to use)

Medium graduated cylinder

Saran wrap

Pour solution into a cold 600 ml beaker (solution should be cloudy). Estimate or use the graduated cylinder to determine the volume. Gently stir in the cold room while slowly adding an equal amount of cold ddH_2O.

Continue to stir for 30 minutes (precipitation of actomyosin).

Centrifuge in the ultracentrifuge rotor T-865 at 20,000 rpm for 1 hr at 4^o C. Alternatively, use the Beckmann 50.2 Ti rotor and spin at 18,400 rpm (both = RCF ~41,000). Be sure you or someone doing the prep is fully trained in the use of the centrifuge, including cleanup and shutting down the machine.

Following the spin, the tubes should have a distinct pellet, a clear middle layer, and a cloudy layer of fat at the top of the tube. Remove the middle-layer supernatant (don't take the fat). You should expect to lose a sizeable portion of the volume you originally added to the tube. Dilute the supernatant with cold ddH_2O 10-fold (i.e. if 100 ml of supernatant, dilute to 1 L).

Cover and let sit for 3-4 hours in the cold room. A distinct layer should form, as in the Day 1 prep. Prepare **buffers D and E** as specified.

Siphon off clear supernatant and centrifuge the rest in SLA-3000 rotor at 8,000 rpm for 15 minutes at 4^o C.

Soak and gently resuspend pellet in about 10 ml **buffer D.**

Dialyze overnight against 2 L **buffer E**, changing the buffer at least once if possible.

Day 3 (5 hours):

Materials:

50 ml beaker

Bucket of ice

10 ml pipette(s)

Saran wrap

Remove the myosin from dialysis, saving a volume of buffer E to later determine protein concentration.

To clarify myosin, spin in the ultracentrifuge rotor T-865 at 20,000 (or 50.2 Ti at 18,400) rpm for 2 hrs at 4° C.

Using a transfer pipette, remove the myosin from the middle layer (leaving the upper fat layer).

Determine the concentration using 3 dilutions (1:25, 1:50, 1:100) and the following:

$((A_{280} - A_{320})/0.55)$ x dilution = _____ mg/ml

Dilute to 50% with cold glycerol by stirring in the cold room. Store at -20C

Buffers

*ATP and DTT are added the morning of the prep

Solutions should be pre-chilled.

Buffer A: Extraction Buffer	**500 ml**
0.3 M KCl	50 ml of 3 M KCl
0.15 M KPi	30.5 ml of 1 M K_2HPO_4
	44.35 ml of 1 M KH_2PO_4
20 mM EDTA	50 ml of 0.2 M EDTA
5 mM $MgCl_2$	510 µl of 4.9 M $MgCl_2$
*3.3 mM ATP	1 g ATP

pH to 6.7

*5 mM DTT		2.5 ml of 1 M DTT, or 0.396 g
	Qs to 500 ml	

Buffer B: Suspension Buffer		**50 ml**
1 M KCl		16.6 ml of 3 M KCl
60 mM KPi		1.5 ml of 1 M K_2HPO_4
		1.5 ml of 1 M KH_2PO_4
20 mM EDTA		5 ml of 0.2 M EDTA
	pH to 6.7	
*5 mM DTT		250 µl of 1 M DTT
	Qs to 50 ml	

Buffer C: Dialysis Buffer		**4 L**
0.6 M KCl		800 ml of 3 M KCl
25 mM KPi		40.8 ml of 1 M K_2HPO_4
		59.2 ml of 1 M KH_2PO_4
	pH to 6.7	
*5 mM DTT		20 ml of 1 M DTT or 3.085 g
	Qs to 4 L	

Buffer D: Resuspension Buffer		**21 ml**
3 M KCl		20 ml of 3 M KCl
50 mM KPi		670 µl of 1 M K_2HPO_4
		330 µl of 1 M $KH_2 PO_4$

	pH to 6.7	
*5 mM DTT		105 µl of 1 M DTT
	Qs to 21 ml	

Buffer E: Dialysis Buffer		**2 L**
0.6 M KCl		400 ml of 3 M KCl
50 mM KPi		58 ml of 1 M K_2HPO_4
		42 ml of 1 M KH_2PO_4
1 mM NaN_3		2 ml of 1 M NaN_3
	pH to 7.0	
*5 mM DTT		10 ml of 1M DTT
	Qs to 2 L	

Stocks

1 M NaN_3	MW = 65.01
0.65 g NaN_3	
Qs to 10 ml	

3 M KCl	MW = 74.55
447.36 g KCl	
2 ml of 1 M NaN_3	
Qs to 2 L	

1 M K_2HPO_4	MW = 174.18

34.84 g K_2HPO_4

200 µl of 1 M NaN_3

Qs to 200 ml

1 M KH_2PO_4 MW = 136.09

27.22 g KH_2PO_4

200 µl of 1 M NaN_3

Qs to 200 ml

1 M $MgCl_2$ MW = 203.3

2.03 g $MgCl_2$

10 µl of 1 M NaN_3

Qs to 10 ml

0.2 M EDTA MW = 292.2

11.69 g EDTA

200 µl of 1 M NaN_3

drip NaOH until dissolved

pH to 8.0

Qs to 200 ml

1 M DTT MW = 154.3

7.715 g DTT

50 µl of 1 M NaN_3

Qs to 50 ml

Protease Inhibitor Cocktail

American Bioanalytical cat# **AB11014**:

AEBSF, Pepstatin A, E-64, Bestatin,

Sodium EDTA

Cold ddH_2O

4 L

APPENDIX B: *In situ* and *In vitro* FORCE PRODUCTION

In Vitro Diaphragm Force Production Protocol

***Protocol based on (Fajardo, V. A., Smith, I. C., Bombardier, E., Chambers, P. J., Quadrilatero, J., & Tupling, A. R. (2016). Diaphragm assessment in mice overexpressing phospholamban in slow-twitch type I muscle fibers. *Brain and behavior*, *6*(6), e00470. https://doi.org/10.1002/brb3.470)

See attached paper for set-up procedure with videos (Moorwood, C., Liu, M., Tian, Z., Barton, E. R. Isometric and Eccentric Force Generation Assessment of Skeletal Muscles Isolated from Murine Models of Muscular Dystrophies. *J. Vis. Exp.* (71), e50036, doi:10.3791/50036 (2013)). Practice of the dissection is crucial for this technique as changes in force development could be a result of technical skill of experimenter, before a study make sure you can consistently produce normal forces. When performing dissection, do so under dissection microscope in cold Tyrodes (also called Ringers) buffer on an ice pack, pining muscle when necessary. Use surgeons' knots to tie off central tendon and loop before attaching to force transducer.

Ensure you bath is filled with Tyrodes solution and oxygenated for 30mins with attached 95% O_2/ 5% CO_2 tank, with water circulator turned on and maintained at 25°C prior to start of surgery. This ensures the bath and muscle has enough oxygen since we are relying on diffusion of oxygen into the muscle and not perfusion through blood supply. CO_2 provides necessary buffering of pH during contraction. Limit strip width to 2mm (maximum 4mm) as wider strips have difficulties with diffusion limitations of O_2. 25°C is used over 37°C as oxygen has poor solubility at higher temperatures.

If you were previously doing in-vivo force

In vitro force is measured in force production (mN) not moment of Force (mN-m)—this is TORQUE

To change units: setup→ Channel set up→ force in device→ select mN

repeat with length (should appear in mm)

setup→ Channel set up →length in → select mm.

Have Bath temperature to 25°C- this is to ensure oxygen stays dissolved in the bath

Protocol:

1. Create folder to save files for each animal→ File→ set up autosave folder→ open folder created→click "current folder"
2. Set up Instant Stim→ this will be used for length optimization and stim optimization.
    a. Pulse Frequency: 1Hz (this is a single twitch; can increase if you want to provide tetanus stimulus)
    b. Pulse width: 0.2ms (how long the stimulus is given)
    c. Number of pulses: 3 (again giving single twitch)
    d. Train Frequency: 0.1Hz (If you are using multiple twitches this gives 10s of rest between stimuli)
    e. Run time: 1 second (amount of time of data collection)

    ** currently I have a better instant stimulation for optimizing current saved (the settings are saved in a photo on force computer)
3. Open live data monitor (File→ open live data monitor); Instant stim orange button will be available for use.
    a. Set time to 10mins (can see protocol or optimization) (screen will automatically scroll)

4. Let diaphragm strip acclimatize for 20-30mins with some tension applied (will appear at 0mm on length in monitor at the end of acclimatization)
    a. This will allow resting tension in the muscle to relax and will reduce background tension; I typically have it resting with some tension on it (6-10mm) and will give it a tetanus stimulus to fully relax the fibres before optimizing length for full data collection.
5. Optimize the current
    a. Range: **1A (50-70%)** (in vitro force stimulation requires a much higher amperage or voltage than in-situ or in-vivo force stimulation since this is a field stimulation- don't be afraid to have it at a high amperage)
    b. Run Instant Stim and check force development.
    c. Increase range to ensure all fibres are recruited- if you see an increase in force development then more fibres have been recruited and you are not at a supramaximal current. Use 3 twitches in a row with increasing current (30s rest between) where force does not increase.
    d. Set supramaximal current by increasing current by 15% (this will ensure you have all fibres being activated in the muscle strip).
6. Optimize the length (necessary to make sure maximal amount of cross bridges are forming)

    YOU NEED TO RECORD THIS LENGTH AT THE END OF DATA COLLECTION
    a. Gradually increase length of diaphragm strip and apply instant stim. Provide 30s of rest to avoid fatigue.
    b. Continue to increase length of diaphragm until you obtain maximal twitch force.

c. You will need to increase the length of the diaphragm quite considerably compared to an upright bath since this bath is flat- but be careful of drastic changes in length this will increase basal tension of diaphragm strip. Use ¼ turns of fine adjustment knob and use gross only when necessary.
d. If you want to collect this data load a single twitch protocol in DMC software and enable autosave- this is optional but for training purposes would be beneficial to look at the shape of the twitch. Can also do this with tetanus to
e. Measure the length of the diaphragm and record, this is L_o and can be input on the main DMC screen and will be used for analysis.
    i. Setup normalization- enter the reference length in mm.
f. Allow some time (approx. 5min) for muscle to rest before starting force frequency curve.

7. Optimal current and length have now been set, protocol is ready to begin.
8. Load "Diaphragm in-vitro force frequency" sequence
    a. Frequencies of 1 Hz, 10Hz, 20Hz, 40Hz, 80Hz, 100 Hz, 120Hz, 140Hz,160Hz & 200Hz
        i. Initial delay: 0.2ms (this is the rest period prior to stim)
        ii. Pulse Frequency: the above frequencies
        iii. Pulse Width: length of stimulus
        iv. Duration: **400ms** (inputted in s in protocol editor) *might consider increasing this but 400ms provides tension to return to baseline recording following contraction (Tupling lab uses a 1 sec- 600-800ms might be sufficient).

b. 60s rest in between; avoids fatigue.

9. Allow 5 mins recovery for the muscle to avoid fatigue in max force test.
10. Load tetanic protocol at the frequency that produces the highest force during force frequency test (label this as pre-fatigue max force test)
11. Perform Pre-Fatigue Max-Force Test
12. Allow 2 mins recovery.
13. Load "**Diaphragm In Vitro Fatigue**" sequence
    a. 70Hz (350ms stim, 0.2ms pulse width) every 2 seconds for 5 mins.
14. Allow 5 minutes recovery from fatigue.
15. Perform a second max force test at the same frequency used in Prefatigue max force test- this assesses recovery from fatigue and can be labelled as **5-min-post-fatigue max** force test.
16. Allow 5 minutes recovery.
17. Perform third max force test; label as **10min-post-fatigue-max.**
18. Allow 5 minutes recovery.
19. Perform Fourth max Recovery test label as **15min-post-fatigue-max.**
20. MAKE SURE YOU HAVE RECORDED LENGTH!!!
21. Remove muscle from bath and remove from central tendon and ribs before weighing. Obtain weight in mg.
22. Data will be normalized to Cross sectional area: mass X length X density
    a. Mammalian skeletal muscle density =1.06g/cm^3 (Mendez and key, 1960); this is commonly used in the field as it. CSA in short allows you to compare differing muscle weights and lengths of muscle. Normalizing to CSA is a way of

controlling for sarcomeres in parallel and normalizing to muscle length during shortening contractions is a way of controlling for the number of sarcomeres in series.

b. “If you need a visual -think of a rope. How strong is a single rope- now cut it in half so you have 2 shorter ropes. Lay them beside each other and glue them together. You now effectively have a new stronger rope with twice the CSA of the first rope, but it weighs the exact same (wait... forget the glue... the rope just really sticky for some reason). Cut the rope again and stick the two pieces together again. Repeat as many times as you want. You now have a rope which has a much larger CSA than the original rope, and it can handle much more load than the original rope but weighs the same and is much shorter. Replace rope with contracting muscle fibres and you probably get the idea.”- Ian Smith 2018

In Situ TA Force Production Protocol

A good rule of thumb is to have practiced this surgery at least 10-15 times and be able to get consistent data with previous literature. If you are doing a new model establish your own normal values in a pilot data set.

Protocol

Create a folder to save files for each animal - Setup: Autosave Folder, open folder you created; click “current folder”

Setup: Instant Stim

Pulse Frequency: 1Hz

Pulse Width: 0.2ms

Number of Pulses: 1

Train Frequency: 0.1Hz

Run Time: 1 second

** I have a train frequency that does 3 twitches with a delay between that I find most useful for optimizing current

Open Live Data monitor and set time to 10 minutes.

Once TA has been sutured at the distal tendon and tied to force transducer, insert needle electrodes in the fascia underneath the TA. Note: do not insert needles directly into muscle belly.

Optimize Current

Range:10mA -100mA (if you can get the right placement this can go to 10mA, but if you struggle can go to 10% of 100mA). If you placed the electrodes well, you will be able to stimulate the sciatic nerve with very little current (20% of 10mA).

Run instant stim.

Adjust range to ensure all muscle fibres are being recruited – obtain 3 twitches in a row where force does not increase (run instant stim and increase current between twitches (wait about 30 seconds in between twitches)

Set supramaximal current by increasing current by 15%

Optimize Resting Length

Increase/decrease length until maximal twitch force is achieved, wait about 30 seconds in between twitches to avoid twitch potentiation.

On average ~10week old female mice have ~10 baseline tension for reference. This can change with age, sex, breed, and disease.

Once optimal current and length have been set, record muscle length and protocol is ready to begin. This step is crucial as the in-situ set-up can have human variability in how high you cut the TA. Recording length ensures consistency.

Load **"TA In Situ Force Frequency"** sequence

Frequencies of 1Hz, 10Hz, 20Hz, 30Hz, 40Hz, 50Hz, 60Hz, 80Hz, 100Hz, 120Hz, 200Hz

Initial Delay: 0.2ms

Pulse Frequency: ____Hz (above frequency)

Pulse Width: 0.2ms

Duration: 300ms

1 minute in between

Harvest muscle and before freezing **MAKE SURE TO RECORD MUSCLE WEIGHT**

Data will be normalized muscle CSA.

APPENDIX C: Preparation of PmFB and Mitochondrial Bioenergetics

Permeabilized Fiber Preparation

Pre-surgery

1. For every fiber bundle you are going to make you will need one 0.5mL tube for wet weights one 1.5mL eppendorf tube for permeabilization and one 1.5mL tube for wash

    * Keep all tubes and buffers on ice

2. In a 5mL tube, make 10mg/mL Saponin solution by dissolving a small amount of saponin in distilled water.
    a. Vortex gently and place on rocker until ready for use
3. Fill all permeabilization tubes with 1.5mL of freshly thawed BIOPS (or BIOPS from fridge with fresh EGTA…see "Other Things to Consider") and *40ug/mL saponin (6uL in 1.5mL BIOPS).
    a. different saponin concentrations may be used depending on species/tissue type but 40ug/mL is standard for rodent.
4. Fill all wash tubes with 1.5mL freshly thawed Buffer Z (or from fridge…same as above)
5. Fill all 0.5mL tubes with 500uL of BIOPS.
6. Using a 50mL falcon tube, weigh out ~ 0.05g of creatine (this number will change based on the number of chambers you need with creatine), add the correct amount of Buffer Z to make a 20mM Creatine Buffer Z Solution
    a. Place on rocker as creatine takes some time to dissolve.
7. Label and fill a 5mL tube with 3.5mL BIOPS for every muscle that will be harvested during surgery.

8. Proceed to “O2k Setup” Section, after O2k’s are setup, you are ready for surgery.

Post-Surgery

1. Separate fibers in BIOPS as quickly and carefully as possible.
    a. Remember to change ice block/ice pack frequently as buffer should never be allowed to warm up.
2. Place separated fibers in corresponding 0.5mL tube with BIOPS and proceed to wet weight procedure.

Bundle Wet Weights

1. Fill a 1.5mL tube with BIOPS until a dome of liquid covers the top.
2. Place tube in holder on scale and tare the scale.
3. With fine forceps remove first bundle from eppendorf and using a kim wipe, blot the bundle to remove excess liquid.
    a. Try to blot no more than 3 times and try to turn the bundle the same way each time to get consistent blotting.
4. Very carefully place bundle in liquid on scale, making sure the forceps to not draw up any liquid.
5. Wait for scale to stabilize and record weight.
6. Until accuracy is proven, do duplicates of each weight and take average if within 0.2mg, repeat weighing if weights are more variable.
7. When done weighing, place back in 0.5mL eppendorf tube until all bundles have been weighed.

Permeabilization

1. Once all bundles are weighed, switch bundles to permeabilization tubes (the ones that have saponin) using forceps or a gel loading pipette tip.
2. Place on nutator in the fridge for 30 minutes.
    a. Make sure all eppendorfs have the liquid mixing by ensuring that the air bubble is moving.
    b. If air bubble appears stuck, invert eppendorf 1-2 times to allow for movement and place back on nutator.
3. After 30 minutes, transfer bundles to corresponding wash tubes using gel loading pipette tip.
4. Place bundles in wash back on nutator in the fridge for 15 minutes.
    a. Permeabilized bundles can remain in fridge in wash for up to 2 hours but will start to lose viability after that point so use bundles ASAP.
5. After 15-minute wash proceed to "Running an Experiment"

Respiration SOP

MOUSE DIA- 20mM Cr				
Substrate	**Event Code**	**STOCK**	**Titration Volume (µL)**	**Final Concentration in Chamber**
Buffer Z Lights Out BLEB Fibre	 F10 BLEB Fibre	20mM Cr 10 mM BLEB	 1	 5 µM
Stop stir bar, turn on lights and verify fibre is in chamber/not stuck on side wall **Hit F10 (lights out)**				
100% O_2	O		Injection	250-275 µM

Pyruvate Malate	P M	**2M** **1M**	**5** **4**	5 mM 2 mM
ADP	25 µM D	**5 mM**	**10**	25 µM
ADP	100 µM D	**50 mM**	**3**	100 µM
ADP	300 µM D	**50 mM**	**8**	300 µM
ADP	500 µM D	**50 mM**	**8**	500 µM
ADP	5 mM D	**500 mM**	**18**	5 mM
ADP	7 mM D	**500 mM**	**8**	7 mM
Glutamate	10 mM G	**2M**	**10**	10 mM
Cyto c	Cyto c	**4 mM**	**5**	10 µM
Succinate	20 mM S	**2M**	**20**	20 mM

MOUSE DIA- No Cr				
Substrate	**Event Code**	**STOCK**	**Titration Volume (µL)**	**Final Concentration in Chamber**
Buffer Z Lights Out BLEB Fibre	 F10 BLEB Fibre	No Cr 10 mM BLEB	 1	 5 µM
Stop stir bar, turn on lights and verify fibre is in chamber/not stuck on side wall **Hit F10 (lights out)**				

100% O_2	O		Injection	250-275 µM
Pyruvate Malate	P M	**2M** **1M**	**5** **4**	5 mM 2 mM
ADP	25 µM D	**5 mM**	**10**	25 µM
ADP	100 µM D	**50 mM**	**3**	100 µM
ADP	300 µM D	**50 mM**	**8**	300 µM
ADP	500 µM D	**50 mM**	**8**	500 µM
ADP	5 mM D	**500 mM**	**18**	5 mM
ADP	7 mM D	**500 mM**	**8**	7 mM
Glutamate	10 mM G	**2M**	**10**	10 mM
Cyto c	Cyto c	**4 mM**	**5**	10 µM
Succinate	20 mM S	**2M**	**20**	20 mM

MOUSE TA- 20mM Cr				
Substrate	**Event Code**	**STOCK**	**Titration Volume (µL)**	**Final Concentration in Chamber**
Buffer Z Lights Out BLEB Fibre	 F10 BLEB Fibre	20mM Cr 10 mM BLEB	 1	 5 µM
Stop stir bar, turn on lights and verify fibre is in chamber/not stuck on side wall **Hit F10 (lights out)**				
100% O_2	O		Injection	250-275 µM
Pyruvate Malate	P M	**2M** **1M**	**5** **4**	5 mM 2 mM
ADP	25 µM D	**5 mM**	**10**	25 µM
ADP	100 µM D	**50 mM**	**3**	100 µM
ADP	300 µM D	**50 mM**	**8**	300 µM
ADP	500 µM D	**50 mM**	**8**	500 µM
ADP	5 mM D	**500 mM**	**18**	5 mM
ADP	7 mM D	**500 mM**	**8**	7 mM
Glutamate	10 mM G	**2M**	**10**	10 mM
Cyto c	Cyto c	**4 mM**	**5**	10 µM
Succinate	20 mM S	**2M**	**20**	20 mM

MOUSE TA- No Cr				
Substrate	**Event Code**	**STOCK**	**Titration Volume (µL)**	**Final Concentration in Chamber**
Buffer Z Lights Out BLEB Fibre	 F10 BLEB Fibre	No Cr 10 mM BLEB	 1	 5 µM
Stop stir bar, turn on lights and verify fibre is in chamber/not stuck on side wall **Hit F10 (lights out)**				
100% O_2	O		Injection	250-275 µM
Pyruvate Malate	P M	**2M** **1M**	**5** **4**	5 mM 2 mM
ADP	25 µM D	**5 mM**	**10**	25 µM
ADP	100 µM D	**50 mM**	**3**	100 µM
ADP	300 µM D	**50 mM**	**8**	300 µM
ADP	500 µM D	**50 mM**	**8**	500 µM
ADP	5 mM D	**500 mM**	**18**	5 mM
ADP	7 mM D	**500 mM**	**8**	7 mM
Glutamate	10 mM G	**2M**	**10**	10 mM
Cyto c	Cyto c	**4 mM**	**5**	10 µM
Succinate	20 mM S	**2M**	**20**	20 mM

MOUSE DIA- 20 mM Cr				
Substrate	**Event Code**	**STOCK**	**Titration Volume (µL)**	**Final Concentration in Chamber**
Buffer Z Lights Out BLEB Fibre	 F10 BLEB Fibre	20 mM Cr 10 mM BLEB	 1	 5 µM
Stop stir bar, turn on lights and verify fibre is in chamber/not stuck on side wall **Hit F10 (lights out)**				
100% O_2	O		Injection	250-275 µM
L-Carnitine Palmitoyl-CoA Malate	L PCoA M	**500mM** **10 mM** **1M**	**20** **4** **1**	5 mM .02 mM .5 mM
ADP	25 µM D	**5 mM**	**10**	25 µM
ADP	100 µM D	**50 mM**	**3**	100 µM
ADP	300 µM D	**50 mM**	**8**	300 µM
ADP	500 µM D	**50 mM**	**8**	500 µM
ADP	5 mM D	**500 mM**	**18**	5 mM
ADP	7 mM D	**500 mM**	**8**	7 mM
Cyto c	Cyto c	**4 mM**	**5**	10 µM
Succinate	20mM S	**2M**	**20**	20mM

MOUSE TA- 20mM Cr

Substrate	Event Code	STOCK	Titration Volume (µL)	Final Concentration in Chamber
Buffer Z Lights Out BLEB Fibre	 F10 BLEB Fibre	20mM Cr 10 mM BLEB	 1	 5 µM
Stop stir bar, turn on lights and verify fibre is in chamber/not stuck on side wall **Hit F10 (lights out)**				
100% O_2	O		Injection	250-275 µM
L-Carnitine Palmitoyl-CoA Malate	L PCoA M	**500mM** **10 mM** **1M**	**20** **4** **1**	5 mM .02 mM .5 mM
ADP	25 µM D	**5 mM**	**10**	25 µM
ADP	100 µM D	**50 mM**	**3**	100 µM
ADP	300 µM D	**50 mM**	**8**	300 µM
ADP	500 µM D	**50 mM**	**8**	500 µM
ADP	5 mM D	**500 mM**	**18**	5 mM
ADP	7 mM D	**500 mM**	**8**	7 mM
Cyto c	Cyto c	**4 mM**	**5**	10 µM
Succinate	20mM S	**2M**	**20**	20mM

mH_2O_2 SOP

- 4 bundles will be made of each tissue (TA and DIA)

PM Protocol:

35uM CDNB (5uL of 10.5mM Stock)

Slot	Assay Buffer	Pre-experiment		Substrate		ADP		ADP		ADP	
1 **(TA or DIA)**	20 mM Creatine AUR 1 mL	**1U HRP** **2 uL** of 500U/mL Fibre	3 min	**10 mM Pyruvate** **5 uL** of 2M **2 mM Malate** **2 uL** of 1M	1 min	**25 uM** **5 uL** of 5 mM	2 min	**100 uM** **1.5 uL** of 50 mM	2 min	**500 uM** **0.8 uL** of 500 mM	2 min
2 **(TA or DIA)**											

Succinate Protocol:

Slot	Assay Buffer	Pre-experiment		Substrate		ADP		ADP		ADP	
1 **(TA or DIA)**	20 mM Creatine AUR 1 mL	**1U HRP** **2 uL** of 500U/mL Fibre	3 min	**10mM Succinate** **5 uL** of 2M	4 min	**25 uM** **5 uL** of 5 mM	2 min	**100 uM** **1.5 uL** of 50 mM	2 min	**500 uM** **0.8 uL** of 500 mM	2 min
2 **(TA or DIA)**	No Creatine AUR 1 mL										

APPENDIX D: Buffers

Buffer Z (Intracellular)

Chemical	Molecular Weight	Final Concentration	Addition to *500mL* Final Volume
K-MES	233.33	105mM	12.26g
KCl	74.55	30mM	1.12g
KH_2PO_4	136.08	10mM	0.7g
$MgCl_2 \cdot 6H_2O$	203.3	5mM	0.51g
EGTA	380.35	1mM	0.19g
BSA		5mg/mL	2.5g

*__ALWAYS__ double check molecular weights for supplier-specific chemicals (n=m/M.W.)

Buffer Z contains the following ion concentrations		**INTRACELLULAR RANGE**
Ca^{2+}	0.0uM	Human: 30nM – 60nM SR: 5.7-20mmol/L Free Ca^{2+} in SR 0.2-0.5mM Rat: 7.76-11.11 ueq/g dry wt

Mg^{2+} (total, not free)	5mM	
Na^{+}	0.0mM	Human: 6-13mM Rat: 7.10-21.9mmol/L
K^{+}	145mM	Human: 130 – 164mmol/L Rat: 117 – 149mmol/L
Cl^{-}	40mM	Rat: 4.97-16.57mmol/L
PO_4^{3-}	10mM	
EGTA free	1mM	

*Buffers do not perfectly reflect extracellular conditions

*Species-specific intracellular ranges exist

*Ranges are expressed as mmol/L (refer to ion concentration summary chart)

To make Buffer Z:

1. Add approximately 400mL of ddH_2O to 1000mL beaker.
2. Weigh and add all powder chemicals.
3. Adjust pH to 7.2 using KOH pellets.
4. Using graduated cylinder, bring total volume to 500mL.
5. Filter and then aliquot into 50mL falcon tubes
6. Freeze falcon tubes

BIOPS Buffer (Extracellular)

Chemical	Stock Solution	Molecular Weight	Final Concentration	Addition to *2 Litre* Final Volume
CaK_2EGTA*	100mM		2.77mM	55.4mL
K_2EGTA*	100mM		7.23mM	144.6mL
Na_2ATP		555.1	5.77mM	6.41g
$MgCl_2 \cdot 6H_2O$		203.3	6.56mM	2.67g
Taurine		125.1	20mM	5.02g
Na_2Phosphocreatine		327.14	15mM	9.81g
Imidazole		68.1	20mM	2.72g
Dithiothreitol (DTT)		154.2	0.5mM	0.154g
MES Hydrate		195.2	50mM	19.52g

*<u>**ALWAYS**</u> double check molecular weights for supplier-specific chemicals (n=m/M.W.)

BIOPS contains the following ion concentrations		**EXTRACELLULAR RANGE**
Ca^{2+} free	0.1uM	<u>Rat:</u> 7.6mM <u>Mouse:</u> 1.3mM
Mg^{2+} free	1mM	

Na^+	41mM	Human: 133-143mM
K^+	20mM	Human: 4.5mM
Cl^-	13mM	Rat: 160mM Mouse: 95-120mM
MgATP	5mM	
Ionic Strength	160mM	
Osmolality	295 mOsm	

*Ionic strength is the sum of all ions

*Buffers do not perfectly reflect extracellular conditions

*Species-specific extracellular ranges exist

*Ranges are expressed as mmol/L (refer to ion concentration summary chart)

CaK_2EGTA: Dissolve 2.002g of $CaCO_3$ in 100mM hot (80°C) solution of EGTA (7.608g of EGTA in 200mL ddH_2O). Add 2.3g of KOH and adjust pH to 7.0 using KOH. Freeze unused portions.

K_2EGTA: Dissolve 7.608g EGTA and 2.3g KOH into 200mL ddH_2O. Adjust pH to 7.0 using KOH. Freeze unused portions.

To make BIOPS:

1. Add approximately 1500mL of ddH_2O to 2000mL beaker.
2. While constantly stirring add stock solutions of CaK_2EGTA and K_2EGTA

3. Weigh and add all powder chemicals.
4. Adjust pH to 7.2 using KOH pellets.
5. Using graduated cylinder, bring total volume to 2000mL.
6. Filter and then aliquot into 50mL falcon tubes
7. Freeze falcon tubes

Amplex Ultra Red – Preparation

Total volume per experiment: 1000ul in Hellma 109.004F fluorescent cell

Total volume per black tube: 1030ul (recommend 1050 next time)

Stock A and B ingredients required:

Amplex Ultra-Red (Invitrogen A36006)

5000 IU/ml Cu/Zn Superoxide dismutase (SOD1; Sigma S9697)

10mM Blebbistatin (BLEB; Cayman)

DMSO

Buffer Z (0.5mg/ml BSA)

0.5M EGTA (aliquots in freezer)

Stock B additional ingredients:

20mM Creatine anhydrous

Final concentrations for both AUR Stock A and AUR Stock B:

10uM AUR

5uM BLEB

25U/ml Cu/Zn SOD1 1mM EGTA

Work fairly quickly given AUR and BLEB should not be stored on ice. Best to prepare with lights out in lab as AUR and BLEB are light sensitive.

Preparation of AUR Stock A (No Creatine):

Step 1: Prepare 5mM AUR. Add 666.6ul of DMSO to 1mg AUR. Vortex gently. Prepare in black tube but do not place on ice (DMSO will freeze).

Step 2: Prepare 10mM BLEB. Add 1.71 ml DMSO to 5mg bottle of BLEB. Prepare in black tube but do not place on ice.

Step 3: Prepare 5000IU/mL SOD1 from 30KU/mL stock. Add 3 mL (ddH2O) to sigma bottle, mix well and move to 15mL falcon tube. Add 3 more mL to sigma bottle again and move this to 15mL falcon tube (6mL altogether). pH this to ~7. **MAKE SURE YOU USE 1M KOH TO BRING pH UP, TITRATE THIS INCREMENTALLY (2uL at a time).** Prepare in 850uL aliquots and keep in freezer labelled with date, name and "5000IU/ml SOD1."

Step 4: Prepare 10uM AUR stock. Mix the following:

- 160.6 ml of Buffer Z (0.5mg/ml BSA). Note: sucrose buffers lower oxidant emission.
- 325ul of 5mM AUR
- 812.5ul of 5000 IU/ml SOD1
- 80.3ul of 10mM BLEB
- 325ul of 0.5M EGTA

Aliquot 1.030 uL in black tubes. Store @ -80°C.

(Recommend 1050 uL next time)

Preparation of AUR Stock B (20mM Creatine):

Prepare 10uM AUR stock as in Stock A but with 20mM creatine anhydrous. Mix the following:

- 160.6 ml of Buffer Z (0.5mg/ml BSA)
- 421.19 mg creatine anhydrous
- 325ul of 5mM AUR
- 812.5ul of 5000 IU/ml SOD1
- 80.3ul of 10mM BLEB
- 325ul of 0.5M EGTA

Aliquot 1.025 uL in black tubes. Store @ -80°C.

(Recommend 1050ul next time)

Ringers Buffer

10X Experimental Stock

Chemical	**Molecular Weight**	**Final Concentration For 10X STOCK**	**Addition to *500mL* final volume**
$NaCl_2$	58.44	1210mM	35.36g
KCl_2	74.55	50mM	1.86g
$MgCl_2 \bullet 6H_2O$	203.30	5mM	0.508g
NaH_2PO_4	120	4mM	0.24g
$NaHCO_3$	84.01	240mM	10.08g
EDTA	292.2	1mM	0.146g

** Freeze stock solution in 50mL Falcon Tubes- thaw when needed in the fridge*

1. Add compounds, in order indicated to 250mL ddH_2O.
2. Bring to final volume (500mL) and stir for several hours- heat if necessary

1M $CaCl_2 \bullet 2H_2O$: Dissolve 7.351g (FW 147.02g/mol) into 50mL ddH_2O and store in fridge in a 50mL Falcon Tube

1X Experimental Solution

Chemical	**Addition to *500mL* final volume**
10X Stock	50mL** **ADD LAST**
1M $CaCl_2$ Stock	900µL
Glucose	0.500g

STEPS:

1. Add 1M $CaCl_2$ stock and glucose to 450mL ddH_2O.
2. Once fully dissolved add stock solution.

   *** this prevents precipitation of Ca^{2+} and phosphate in the stock solution

   -pH of experiment solution will be approximately 7.3 while bubbling with 5% CO_2/95% O_2